

# S-Geranylgeranyl-L-glutathione is a ligand for human B cell-confinement receptor P2RY8

Erick Lu<sup>1</sup>, Finn D. Wolfreys<sup>1</sup>, Jagan R. Muppidi<sup>1,2</sup>, Ying Xu<sup>1</sup> & Jason G. Cyster<sup>1\*</sup>

**Germinal centres are important sites for antibody diversification and affinity maturation, and are also a common origin of B cell malignancies. Despite being made up of motile cells, germinal centres are tightly confined within B cell follicles. The cues that promote this confinement are incompletely understood. P2RY8 is a G $\alpha_{13}$ -coupled receptor that mediates the inhibition of migration and regulates the growth of B cells in lymphoid tissues<sup>1,2</sup>. P2RY8 is frequently mutated in germinal-centre B cell-like diffuse large B cell lymphoma (GCB-DLBCL) and Burkitt lymphoma<sup>1,3–6</sup>, and the ligand for this receptor has not yet been identified. Here we perform a search for P2RY8 ligands and find P2RY8 bioactivity in bile and in culture supernatants of several mouse and human cell lines. Using a seven-step biochemical fractionation procedure and a drop-out mass spectrometry approach, we show that a previously undescribed biomolecule, S-geranylgeranyl-L-glutathione (GGG), is a potent P2RY8 ligand that is detectable in lymphoid tissues at the nanomolar level. GGG inhibited the chemokine-mediated migration of human germinal-centre B cells and T follicular helper cells, and antagonized the induction of phosphorylated AKT in germinal-centre B cells. We also found that the enzyme gamma-glutamyltransferase-5 (GGT5), which was highly expressed by follicular dendritic cells, metabolized GGG to a form that did not activate the receptor. Overexpression of GGT5 disrupted the ability of P2RY8 to promote B cell confinement to germinal centres, which indicates that GGT5 establishes a GGG gradient in lymphoid tissues. This work defines GGG as an intercellular signalling molecule that is involved in organizing and controlling germinal-centre responses. As the P2RY8 locus is modified in several other types of cancer in addition to GCB-DLBCL and Burkitt lymphoma, we speculate that GGG might have organizing and growth-regulatory roles in multiple human tissues.**

To establish a bioassay for P2RY8, we used the inferred ability of P2RY8 to support the inhibition of cell migration<sup>1</sup>. P2RY8 was expressed in a lymphoid cell line (WEHI-231) and the highest-expressing cells were selected to maximize ligand sensitivity. Extracts were prepared from mouse tissues and tested for their ability to inhibit P2RY8<sup>+</sup> cell migration towards a chemokine, CXCL12 (Fig. 1a). We detected bioactivity in extracts from the liver, but not in extracts from the spleen, lymph nodes, thymus, brain, kidney or serum. Further analysis of hepatic tissues revealed that bile was a more potent source of activity (Fig. 1b).

We then found that several adherent cell lines also produced bioactivity (Fig. 1c). The presence of bioactivity in the culture supernatants was enhanced by the inclusion of albumin in the medium (Extended Data Fig. 1a). Separation of molecules that were greater than 50 kDa in size from those that were less than 50 kDa in size (bovine albumin is approximately 66.5 kDa in size) revealed that bioactivity was enriched in the >50-kDa fraction (Extended Data Fig. 1b). However, bioactivity could be extracted from the protein precipitate using methanol, which suggests that the bioactive compound was a metabolite that was associated with albumin (Extended Data Fig. 1c). Using a Folch extraction method, the bioactivity partitioned with the methanol–water

layer, suggesting that the compound could be a polar lipid (Extended Data Fig. 1d).

Given this result, we asked whether inhibitors of lipid biosynthesis affected the production of bioactivity. Inhibitors of phospholipase, lipoxygenase and cyclooxygenase did not have an effect (Extended Data Fig. 1e), but statins caused a marked reduction in the production of bioactivity (Fig. 1d and Extended Data Fig. 1f). Bioactivity production could be rescued by supplying statin-treated cells with mevalonate or geranylgeranyl-pyrophosphate (GG-PP), which suggested that the isoprenoid biosynthesis pathway contributed to ligand generation (Fig. 1d).

We developed a high-performance liquid chromatography (HPLC) fractionation procedure to purify the bioactive compound from bile and culture supernatants, and used mass spectrometry to identify molecules that were common to the active fractions (Fig. 1e and Extended Data Fig. 2a, b). We also performed a drop-out mass spectrometry analysis of side-by-side purified supernatants from control and statin-treated Hepa 1-6 cells. The purified fractions were analysed using positive-ion-mode Q1 mass spectrometry scans, which identified a single ion with a  $m/z$  value of 580.3 that was enriched in bioactive fractions and absent from the corresponding statin-treated fraction (Fig. 1f). Negative-ion-mode scans revealed drop-out of an ion with a  $m/z$  of 578.3 (Extended Data Fig. 2c). Given the two-unit difference in the  $m/z$  value, the positive-ion and negative-ion candidates could be assigned, respectively, to  $[M + H]^+$  and  $[M - H]^-$  ions of the same molecule. High-resolution liquid chromatography–mass spectrometry (LC–MS) identified a positive ion with a  $m/z$  of 580.3435 (Extended Data Fig. 3a).

A positive ion with a  $m/z$  of 580.3435 did not match any known biological molecules in metabolite databases. Fragmentation of this ion produced a tandem mass spectrometry (MS/MS) spectrum that was similar to that of glutathione<sup>7,8</sup> (Extended Data Fig. 3b). Subtracting the monoisotopic mass of a glutathione conjugate from 580.3435 and accounting for the positive proton adduct yielded a monoisotopic mass of 274.2674—potentially corresponding to a chemical formula of C<sub>20</sub>H<sub>34</sub>. This matched geranylgeranyl, an isoprenoid produced by cells in the form of GG-PP<sup>9</sup>. Comparison of the MS/MS spectra of GG-PP with the candidate ion revealed a shared product ion with a  $m/z$  value of 273.1 that produced similar MS/MS spectra and potentially corresponded to a geranylgeranyl ion (Extended Data Fig. 3c).

Next, we chemically synthesized GGG, the glutathione-S-conjugate of geranylgeranyl (Fig. 1g). This compound had the same elution profile, mass and fragmentation pattern as the  $m/z$  580.3435 ion of purified bile (Fig. 1h and Extended Data Fig. 3d, e). Using our synthesized GGG as a reference standard, we developed an LC–MS/MS method to quantify the levels of GGG in tissues. We detected low nanomolar amounts of GGG in extracts from mouse spleen, mouse lymph nodes and human tonsil, and low micromolar levels in mouse bile (Fig. 1i). Concentrated extracts from mouse spleen and human tonsil also showed P2RY8 bioactivity (Fig. 1j).

<sup>1</sup>Howard Hughes Medical Institute and Department of Microbiology and Immunology, University of California, San Francisco, CA, USA. <sup>2</sup>Present address: Lymphoid Malignancies Branch, National Cancer Institute, National Institutes of Health, Bethesda, MD, USA. \*e-mail: [jason.cyster@ucsf.edu](mailto:jason.cyster@ucsf.edu)

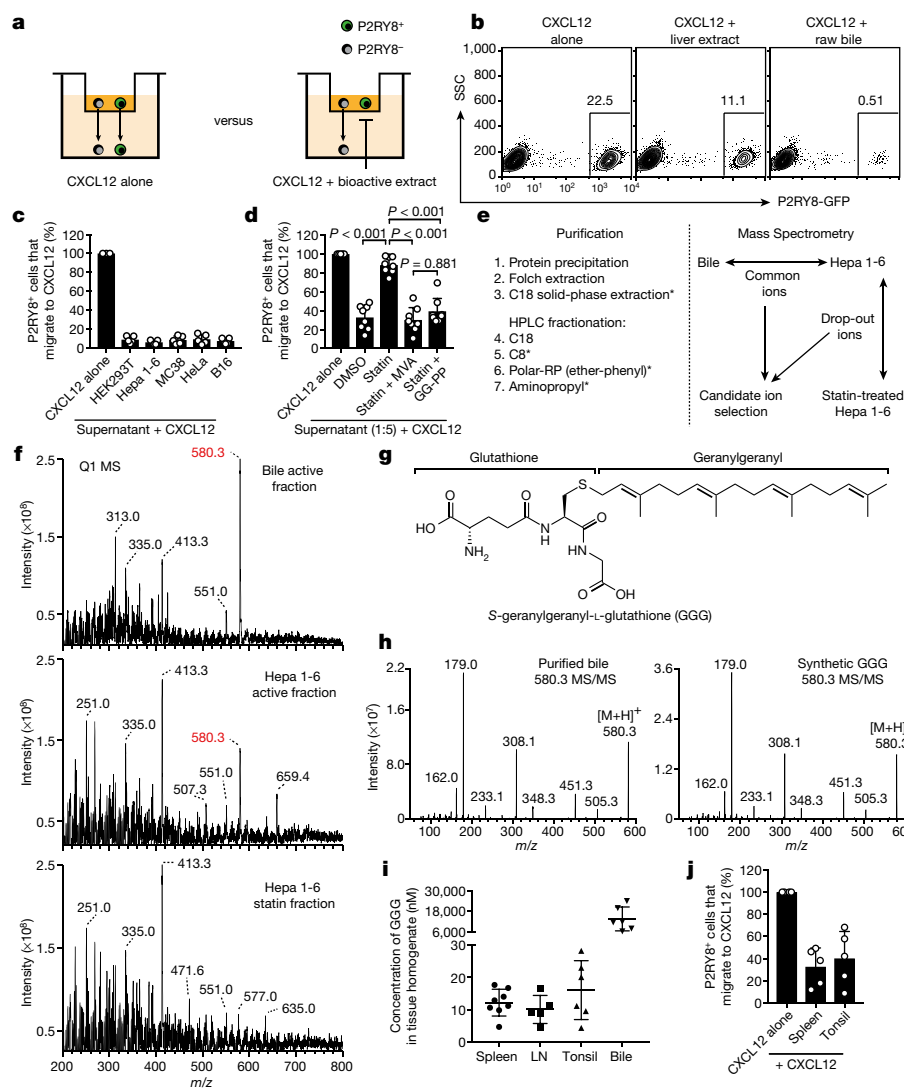


**Fig. 1 | Purification and identification of GGG as an endogenous compound that activates P2RY8.** **a**, Diagram of transwell P2RY8 ligand bioassay, showing that migration of P2RY8<sup>+</sup> WEHI-231 cells (green) is inhibited by extracts containing P2RY8 ligand. **b**, Flow cytometry plots of cells from the bottom well of the bioassay described in **a**, using mouse liver extract or diluted bile. **c**, P2RY8 ligand bioassay of culture medium from the indicated cell lines ( $n = 5$ ). **d**, P2RY8 ligand bioassay of medium from Hepa 1-6 cells incubated with the indicated agents (10  $\mu$ M statin, 100  $\mu$ M mevalonate (MVA), 100  $\mu$ M GG-PP or dimethyl sulfoxide (DMSO) vehicle) ( $n = 8$ ,  $P$  values determined by one-way analysis of variance (ANOVA) with Bonferroni's multiple comparisons test). **e**, Left, diagram of the seven-step purification strategy used to identify the bioactive compound in bile. Asterisks indicate steps used for culture supernatants.

GGG inhibited migration of P2RY8<sup>+</sup> but not P2RY8<sup>-</sup> cells towards CXCL12 and a second chemokine, CXCL13, and showed maximal inhibitory activity at concentrations of 10–100 nM (Fig. 2a and Extended Data Fig. 4a, b). By contrast, GGG did not have an inhibitory effect on migration for several other receptors that can couple to G $\alpha_{13}$ , including S1PR2 and GPR4<sup>10</sup> (Extended Data Fig. 4a, c). GGG was potent in inhibiting the migration of tonsil germinal-centre B cells, but had a weaker effect on naive B cells (Fig. 2b)—consistent with their lower P2RY8 expression (Extended Data Fig. 5a). Human T follicular helper (T<sub>FH</sub>) cells also express P2RY8 (Extended Data Fig. 5a), and GGG was inhibitory for their migration, although with less potency than for germinal-centre B cells (Fig. 2c). Leukotriene C<sub>4</sub> (LTC<sub>4</sub>)—a ligand for CYSLTR1 and CYSLTR2—is a glutathione-lipid conjugate derived from arachidonic acid, and is produced by a distinct pathway compared with geranylgeranyl<sup>11</sup>. LTC<sub>4</sub> had a

measurable effect on P2RY8, but with 100-fold lower potency than GGG (Fig. 2a). GGG promoted internalization of P2RY8, but not of other receptors, including S1PR2, GPR55, CYSLTR1 and CYSLTR2 (Fig. 2d). These findings demonstrate that GGG is a potent and selective P2RY8 ligand. Staining of tonsil tissue showed that P2RY8 was present throughout the germinal centre and expressed at a higher level in a subset of germinal-centre-associated cells (Extended Data Fig. 5b). Many of the P2RY8<sup>high</sup> cells co-stained for CD4, although not all germinal-centre-associated CD4<sup>+</sup> cells were P2RY8<sup>high</sup> (Extended Data Fig. 5b). Intracellular flow cytometry with the C-terminus-specific anti-P2RY8 antibody revealed expression of P2RY8 in germinal-centre B cells and T<sub>FH</sub> cells (Extended Data Fig. 5c, d). Consistent with the microscopy data, a subset of the T<sub>FH</sub> cells had high P2RY8 expression (Extended Data Fig. 5d). P2RY8<sup>high</sup>CD4<sup>+</sup> T cells were not observed outside

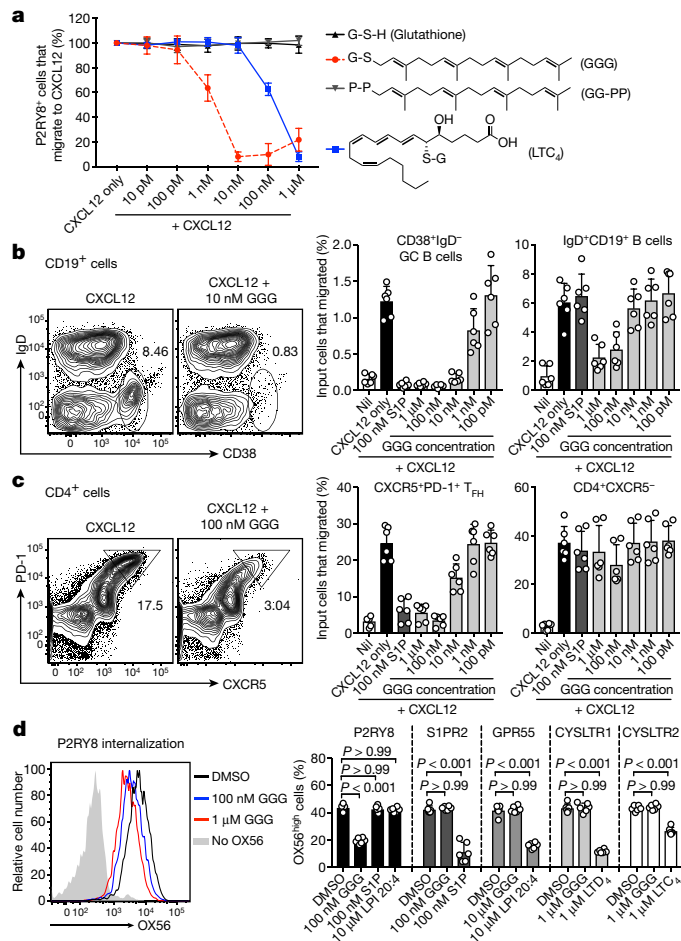


**Fig. 2 | GGG inhibits the migration of P2RY8-expressing cells.** **a**, P2RY8 ligand bioassay (45 min, 37 °C) using the indicated concentrations of GGG, glutathione, GG-PP or LTC<sub>4</sub>, with 50 ng ml<sup>-1</sup> CXCL12 (*n* = 4 biological replicates). **b**, **c**, Transwell migration assays of human tonsil cells towards CXCL12 mixed with the indicated concentrations of GGG. Left, representative flow cytometry plots of CD19<sup>+</sup> cells (**b**), showing the gate for CD38<sup>+</sup>IgD<sup>-</sup> germinal-centre (GC) B cells, or of CD4<sup>+</sup> cells (**c**), showing the gate for PD-1<sup>+</sup>CXCR5<sup>+</sup>T<sub>FH</sub> cells. Right, graphs summarizing the data for indicated cell types (*n* = 3 tonsils, two technical replicates each). **d**, Internalization assay using cells expressing OX56 epitope-tagged P2RY8, read by measuring surface OX56 levels. Left, representative flow cytometry histogram. Right, graphs summarizing the data for the indicated receptors (*n* = 6 biological replicates, *P* values determined by one-way ANOVA with Bonferroni's multiple comparisons test). Data are pooled from three experiments (**a–d**). Graphs depict mean with s.d. and points represent biological replicates.

germinal centres, in keeping with the notion that high receptor expression confines cells to the germinal centre.

The frequent mutation of P2RY8 in GCB-DLBCL and Burkitt lymphoma is thought to reflect an ability of the receptor to function, analogously to S1PR2, as a repressor of AKT activation<sup>1,12,13</sup>. In accordance with this model, GGG antagonized chemokine-induced phosphorylated AKT (pAKT) in GCB-DLBCL lines with intact P2RY8 and GNA13 genes (Fig. 3a, b). To confirm that GGG was acting via endogenously expressed P2RY8, we used CRISPR-Cas9-mediated gene editing to generate a line of Ly8 cells in which approximately 80% of P2RY8 alleles were mutated (Extended Data Fig. 5e, f). In P2RY8-mutated cells, GGG no longer caused inhibition of CXCL12-mediated pAKT induction or migration (Fig. 3c, d). Moreover, restoration of G<sub>α13</sub> expression in the GNA13 mutant DOHH2 cell line rescued the ability of GGG to repress pAKT (Extended Data Fig. 5g). GGG also antagonized pAKT induction in P2RY8-transduced WEHI-231 cells, without affecting control P2RY8<sup>-</sup> cells (Extended Data Fig. 5h).

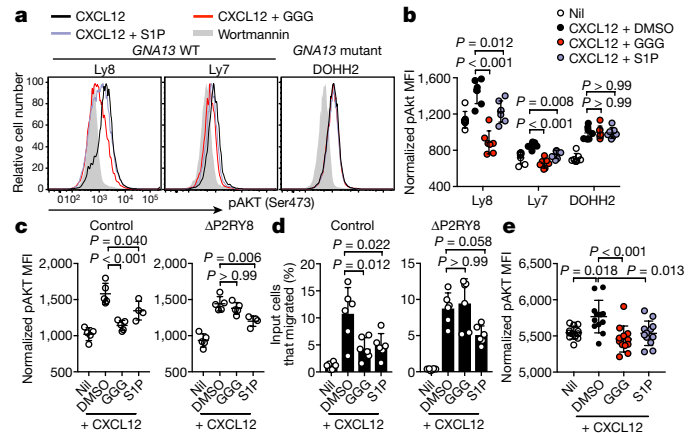


**Fig. 3 | GGG suppresses chemokine-induced AKT phosphorylation in cell lines and tonsil germinal-centre B cells.** **a**, **b**, Representative histograms (**a**) and summary data (**b**) showing pAKT levels in the indicated DLBCL lines treated with wortmannin (grey fill), CXCL12 (black), CXCL12 + S1P (blue) or CXCL12 + GGG (red) (*n* = 7). MFI, mean fluorescence intensity; WT, wild type. **c**, pAKT levels in Ly8 cells edited using CRISPR-Cas9 with either a control guide or a guide targeting P2RY8 (ΔP2RY8), treated as in **a** (*n* = 5, *n* = 4 for S1P). **d**, Transwell migration assay using gene-edited Ly8 cells towards 5 ng ml<sup>-1</sup> CXCL12, along with 100 nM GGG, 100 nM S1P or vehicle (*n* = 6). **e**, pAKT levels in tonsil germinal-centre B cells, treated as indicated (*n* = 6 tonsils, two replicates each). pAKT MFI data were normalized based on the nil condition. Data are representative of, or pooled from, four (**a**, **b**, **e**) or three (**c**, **d**) experiments. Graphs depict mean with s.d. and points represent biological replicates. *P* values determined by one-way ANOVA with Bonferroni's multiple comparisons test (**b–e**).

Notably, GGG antagonized pAKT induction in tonsil germinal-centre B cells to an extent similar to that caused by sphingosine-1-phosphate (S1P) (Fig. 3g).

We speculated that GGG, as a glutathione conjugate, might be metabolized by enzymes of the γ-glutamyltransferase class<sup>14</sup>. We therefore tested the ability of this enzyme class to antagonize the production of P2RY8 bioactivity in cell lines. Overexpression of GGT5 (also known as γ-glutamyl leukotrienase owing to its ability to metabolize LTC<sub>4</sub> to LTD<sub>4</sub><sup>15,16</sup>) caused a loss of bioactivity in culture supernatants (Fig. 4a, b). Moreover, GGT5-expressing cells were capable of inactivating synthetic GGG (Fig. 4b). The other mouse GGT family members—as well as GGT2, a human GGT—had either weak or no activity in metabolizing GGG (Extended Data Fig. 6a). We hypothesized that GGT5 was cleaving the γ-glutamyl moiety off GGG to form S-geranylgeranyl-L-Cys-Gly (Fig. 4c), with a resulting loss of 129 Da. Indeed, transfection of HEK293T cells with GGT5 caused the conversion of synthetic GGG (*m/z* 580.3) to its predicted Cys-Gly metabolite (*m/z* 451.3) (Fig. 4d and Extended Data Fig. 6b). We detected LC-MS/MS signals corresponding to the Cys-Gly metabolite in extracts from mouse spleen (Fig. 4e), which suggests that this metabolic process occurs *in vivo*.

Gain-of-function studies in mice have shown that P2RY8 promotes the positioning of B cells in the centre of follicles<sup>1,2</sup>. We therefore predicted that GGG would be strongly metabolized in the follicle centre, resulting in higher levels of GGG in the outer areas and confinement of P2RY8<sup>+</sup> cells to the central region. Consistent with this model, Protein Atlas data provided evidence that GGT5 was expressed in germinal centres in human tonsil and lymph nodes<sup>17</sup>. Our tonsil tissue staining showed that GGT5 was expressed in a pattern that aligned with the follicular dendritic cell (FDC) marker, CR2 (Fig. 4f and Extended Data Fig. 6c). Co-staining confirmed that GGT5 was expressed by CR2<sup>+</sup> FDCs but not by germinal-centre B cells (Extended Data Fig. 6d), and quantitative polymerase chain reaction (qPCR) analysis showed high GGT5 expression in tonsil stroma (Extended Data Fig. 6e). A single-cell RNA sequencing analysis of mouse lymph node stromal cells<sup>18</sup> showed

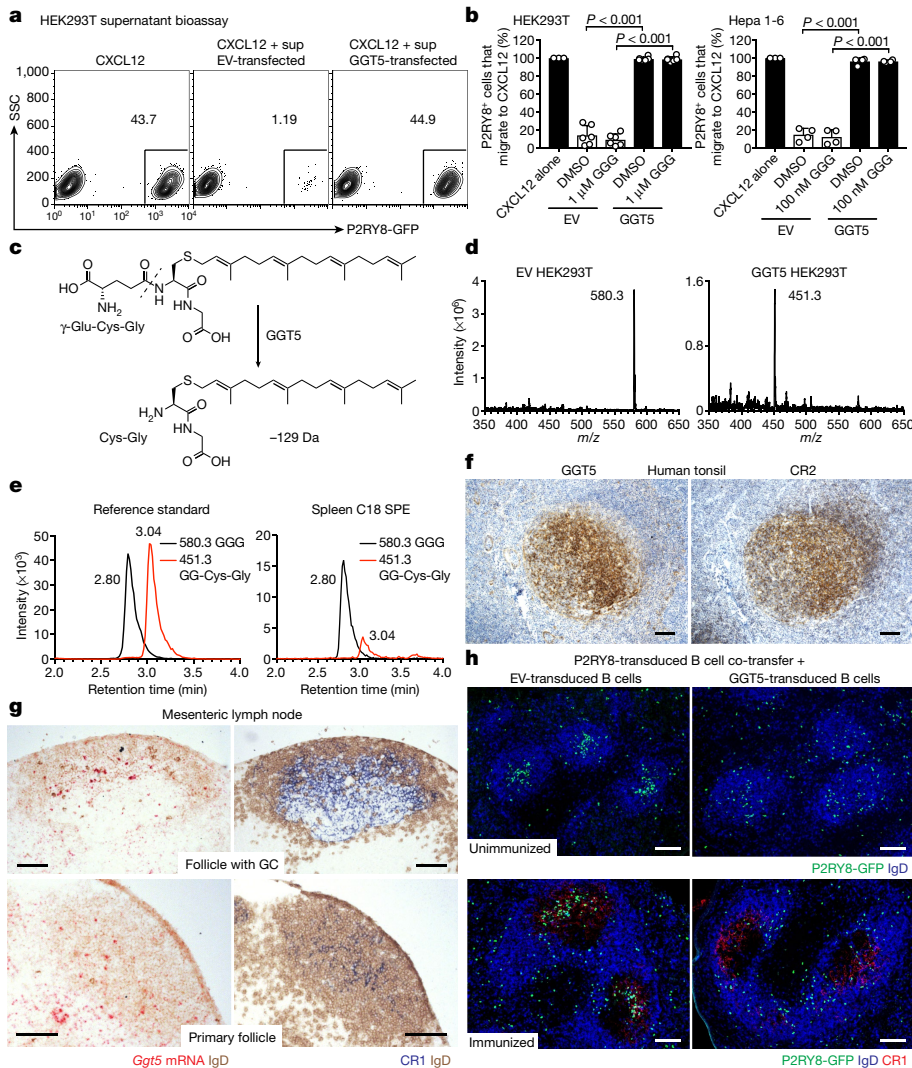


**Fig. 4 | GGT5 metabolizes GGG and regulates P2RY8 function in vivo.** **a, b**, Flow cytometry plots (**a**) and summary data (**b**) of P2RY8 ligand bioassay of supernatants (sup) from the indicated cells overexpressing GGT5 or empty vector (EV), cultured for 18 h with GGG or vehicle (HEK293T  $n = 6$ , Hepa 1-6  $n = 4$  biological replicates,  $P$  values determined by one-way ANOVA with Bonferroni's multiple comparisons test). Graphs depict mean with s.d. **c**, Diagram of GGG conversion into S-geranylgeranyl-L-Cys-Gly (GG-Cys-Gly). **d**, Positive precursor ion scan for  $m/z$  179 to identify ions producing [Cys-Gly] $^+$  fragments, from purified supernatants of HEK293T cells overexpressing empty vector or GGT5, and incubated with 10  $\mu$ M GGG. **e**, LC-MS/MS multiple reaction monitoring scans for GGG and GG-Cys-Gly in a mixture of 100 nM GGG and GG-Cys-Gly, or in C18 solid-phase extraction concentrates of

mouse spleen. **f**, Immunohistochemistry for GGT5 or CR2 (brown) in serial sections of tonsil counterstained with haematoxylin (blue). **g**, RNAscope for *Ggt5* mRNA (red) in mouse lymph node germinal centres and primary follicles, counterstained with IgD (brown). Serial sections were stained for CR1 (blue) and IgD (brown). **h**, Immunofluorescence for P2RY8-overexpressing B cells (green fluorescent protein (GFP), green) co-transferred with empty vector or GGT5-overexpressing B cells, in unimmunized mice without germinal centres (top), and in germinal centres (CR1, red) of immunized mice (bottom), relative to endogenous B cells (IgD, blue). Data are representative of, or pooled from, three (**a, b, e**) or two (**d**) experiments; or three (**f, g**) biological repeats. Scale bars, 100  $\mu$ m.

that GGT5—but not GGT1, GGT6 or GGT7—was enriched in FDCs (Extended Data Fig. 7a). qPCR also demonstrated that GGT5 was enriched in spleen stroma (Extended Data Fig. 7b), and previous RNA-seq analysis has shown that the GGT family is minimally expressed in germinal-centre B cells (www.immgen.org). We also performed in situ hybridization, which revealed that *Ggt5* was expressed in mouse germinal centres and primary follicles in a pattern similar to CR1 $^+$  FDCs (Fig. 4g and Extended Data Fig. 7c). In both human and mouse tissue, expression was evident in some high endothelial venules, consistent with microarray data<sup>19</sup>; lower levels of expression were detectable in the T zone and expression was minimal in the outer regions of lymphoid follicles (Fig. 4f, g and Extended Data Figs. 6c, 7c). Treatment of mice with lymphotoxin  $\beta$  receptor (LT $\beta$ R)-Fc and tumour necrosis factor receptor-Fc fusion proteins to ablate FDCs<sup>20</sup> caused loss of *Ggt5* in germinal centres (Extended Data Fig. 7d).

We hypothesized that if GGT5 were involved in establishing GGG gradients, then increasing the expression of GGT5 throughout the follicle should disrupt the gradient and thus compromise the ability of P2RY8 to confine cells to the follicle centre. To test this idea, P2RY8-expressing B cells were transferred into mice along with large numbers of GGT5-expressing B cells or, as a control, empty-vector-expressing B cells. In the control recipients, P2RY8 caused B cells to localize within pre-existing germinal centres or in the central region of follicles that lacked germinal centres (Fig. 4h and Extended Data Fig. 8a, b), as expected<sup>1</sup>. By contrast, in recipients of GGT5-expressing B cells, P2RY8 no longer caused B cell confinement to the germinal centre or follicle centre (Fig. 4h and Extended Data Fig. 8a, b). The GGT5-expressing B cells were scattered through the follicle and did not display altered positioning compared with control B cells (Extended Data Fig. 8c). These data provide in vivo evidence that GGT5 controls P2RY8 ligand

distribution, and corroborate the finding that FDCs are required for the function of P2RY8 as a B cell-confinement receptor<sup>2</sup>.

P2RY8 is mutated in up to 20% of cases of GCB-DLBCL and Burkitt lymphoma, as well as in some transforming follicular lymphomas<sup>1,3–6,21</sup>, which provides strong evidence that the receptor and its ligand have an essential, non-redundant constraining function in human germinal-centre B cells. In this study, we identified GGG as an intercellular signalling molecule that activates P2RY8 to exert inhibitory effects on cell migration and growth. The low abundance of GGG in lymphoid tissue is consistent with the nanomolar potency of GGG as a P2RY8 ligand, and with the localized metabolism of GGG that establishes organizing gradients. Our data indicate that albumin serves as a carrier for GGG, and we hypothesize that stromal cells in the outer regions of follicles are a source of extracellular GGG. We do not have an explanation for the abundance of GGG in bile, but it may indicate that GGG has a role in the hepatobiliary system. There are approximately 25 glutathione transferases that can conjugate glutathione to target molecules<sup>16</sup> and many of these are expressed in lymphoid tissues ([www.immgen.org](http://www.immgen.org)). Future studies will be needed to define the biosynthetic pathway for GGG. P2RY8 is downregulated in memory B cells and plasma cells<sup>22</sup>, and this may help these cells exit from germinal centres. Although P2RY8 is widely conserved in vertebrates, it is, notably, not present in rodents<sup>1</sup>. We speculate that a non-orthologous GGG receptor may exist in the mouse. Given that P2RY8 could respond to both GGG and LTC<sub>4</sub>, P2RY8 or P2RY8-like receptors may be able to sense a range of glutathione-conjugated lipids. Our studies raise the possibility that GGG derivatives might be useful as suppressors of germinal-centre B cell growth—for example, in cases of P2RY8<sup>+</sup> DLBCL or Burkitt lymphoma. As GGG is made by multiple tumour cell lines and the P2RY8 locus is modified in some other cancer types such as acute lymphoblastic leukaemia<sup>23</sup>, prostate cancer and stomach cancer ([www.cbioportal.org](http://www.cbioportal.org) and [www.intogen.org](http://www.intogen.org)), we reason that GGG may have organizational and growth-regulatory functions in several human tissues.

### Online content

Any methods, additional references, Nature Research reporting summaries, source data, statements of data availability and associated accession codes are available at <https://doi.org/10.1038/s41586-019-1003-z>.

Received: 16 September 2018; Accepted: 28 January 2019;  
Published online: 06 March 2019

- Muppidi, J. R. et al. Loss of signalling via G $\alpha$ 13 in germinal centre B-cell-derived lymphoma. *Nature* **516**, 254–258 (2014).
- Muppidi, J. R., Lu, E. & Cyster, J. G. The G protein-coupled receptor P2RY8 and follicular dendritic cells promote germinal center confinement of B cells, whereas S1PR3 can contribute to their dissemination. *J. Exp. Med.* **212**, 2213–2222 (2015).
- Lohr, J. G. et al. Discovery and prioritization of somatic mutations in diffuse large B-cell lymphoma (DLBCL) by whole-exome sequencing. *Proc. Natl Acad. Sci. USA* **109**, 3879–3884 (2012).
- Morin, R. D. et al. Mutational and structural analysis of diffuse large B-cell lymphoma using whole-genome sequencing. *Blood* **122**, 1256–1265 (2013).
- Forbes, S. A. et al. COSMIC: mining complete cancer genomes in the Catalogue of Somatic Mutations in Cancer. *Nucleic Acids Res.* **39**, D945–D950 (2011).
- Schmitz, R. et al. Genetics and pathogenesis of diffuse large B-cell lymphoma. *N. Engl. J. Med.* **378**, 1396–1407 (2018).
- Dieckhaus, C. M., Fernández-Metzler, C. L., King, R., Krolkowski, P. H. & Baillie, T. A. Negative ion tandem mass spectrometry for the detection of glutathione conjugates. *Chem. Res. Toxicol.* **18**, 630–638 (2005).
- Xie, C., Zhong, D. & Chen, X. A fragmentation-based method for the differentiation of glutathione conjugates by high-resolution mass spectrometry with electrospray ionization. *Anal. Chim. Acta* **788**, 89–98 (2013).

- Wiemer, A. J., Wiemer, D. F. & Hohl, R. J. Geranylgeranyl diphosphate synthase: an emerging therapeutic target. *Clin. Pharmacol. Ther.* **90**, 804–812 (2011).
- Justus, C. R. & Yang, L. V. GPR4 decreases B16F10 melanoma cell spreading and regulates focal adhesion dynamics through the G $\beta$ 13/Rho signaling pathway. *Exp. Cell Res.* **334**, 100–113 (2015).
- Shimizu, T. Lipid mediators in health and disease: enzymes and receptors as therapeutic targets for the regulation of immunity and inflammation. *Annu. Rev. Pharmacol. Toxicol.* **49**, 123–150 (2009).
- Green, J. A. et al. The sphingosine 1-phosphate receptor S1P<sub>2</sub> maintains the homeostasis of germinal center B cells and promotes niche confinement. *Nat. Immunol.* **12**, 672–680 (2011).
- Green, J. A. & Cyster, J. G. S1PR2 links germinal center confinement and growth regulation. *Immunity Rev.* **247**, 36–51 (2012).
- Heisterkamp, N., Groffen, J., Warburton, D. & Sneddon, T. P. The human gamma-glutamyltransferase gene family. *Hum. Genet.* **123**, 321–332 (2008).
- Carter, B. Z. et al. Metabolism of leukotriene C<sub>4</sub> in gamma-glutamyl transpeptidase-deficient mice. *J. Biol. Chem.* **272**, 12305–12310 (1997).
- Hayes, J. D., Flanagan, J. U. & Jowsey, I. R. Glutathione transferases. *Annu. Rev. Pharmacol. Toxicol.* **45**, 51–88 (2005).
- Uhlén, M. et al. Proteomics. Tissue-based map of the human proteome. *Science* **347**, 1260419 (2015).
- Rodda, L. B. et al. Single-cell RNA sequencing of lymph node stromal cells reveals niche-associated heterogeneity. *Immunity* **48**, 1014–1028.e6 (2018).
- Lee, M. et al. Transcriptional programs of lymphoid tissue capillary and high endothelium reveal control mechanisms for lymphocyte homing. *Nat. Immunol.* **15**, 982–995 (2014).
- Allen, C. D. & Cyster, J. G. Follicular dendritic cell networks of primary follicles and germinal centers: phenotype and function. *Semin. Immunol.* **20**, 14–25 (2008).
- Kridel, R. et al. Histological transformation and progression in follicular lymphoma: a clonal evolution study. *PLoS Med.* **13**, e1002197 (2016).
- Brune, V. et al. Origin and pathogenesis of nodular lymphocyte-predominant Hodgkin lymphoma as revealed by global gene expression analysis. *J. Exp. Med.* **205**, 2251–2268 (2008).
- Mullighan, C. G. et al. Rearrangement of *CRLF2* in B-progenitor- and Down syndrome-associated acute lymphoblastic leukemia. *Nat. Genet.* **41**, 1243–1246 (2009).

**Acknowledgements** We thank E. Bess and P. Turnbaugh for providing access to their HPLC equipment; Z. Zhang and K. Shokat for providing access to their chemistry equipment and quadrupole time-of-flight mass spectrometer; J. Jespersen and J. Baron for helping to coordinate tonsil specimens; L. Staudt for DLBCL cell lines; N. Barclay for the OX56 hybridoma; J. An for assistance with mouse husbandry; and D. Russell, J. McDonald and J. Wu for discussions. J.G.C. is an investigator of the Howard Hughes Medical Institute. E.L. was supported by the UCSF Biomedical Sciences Graduate Program and NSF grant 1144247. This work was supported in part by NIH grant RO1 AI45073.

**Reviewer information** Nature thanks Charles Mackay, Michel Nussenzweig and Hai Qi for their contribution to the peer review of this work.

**Author contributions** E.L., J.R.M. and J.G.C. conceptualized the project. E.L. and J.G.C. designed the experiments, interpreted the results and wrote the manuscript. E.L. performed the experiments. F.D.W. chemically synthesized GGG, acquired high-resolution mass spectrometry data and edited the manuscript. Y.X. cloned enzymes and performed qPCR experiments. J.R.M. cloned OX56-tagged receptors and edited the manuscript.

**Competing interests** The authors declare no competing interests.

### Additional information

**Extended data** is available for this paper at <https://doi.org/10.1038/s41586-019-1003-z>.

**Supplementary information** is available for this paper at <https://doi.org/10.1038/s41586-019-1003-z>.

**Reprints and permissions information** is available at <http://www.nature.com/reprints>.

**Correspondence and requests for materials** should be addressed to J.G.C.  
**Publisher's note:** Springer Nature remains neutral with regard to jurisdictional claims in published maps and institutional affiliations.

© This is a U.S. government work and not under copyright protection in the U.S.; foreign copyright protection may apply 2019

## METHODS

**Mice and treatments.** C57BL/6J mice were bred in an internal colony and 7–12-week-old mice of both sexes were used. *Cd19*<sup>-/-</sup> mice on a B6 background were from Jax. Littermate controls were used for experiments, mice were allocated to control and experimental groups randomly, sample sizes were chosen based on previous experience to obtain reproducible results and the investigators were not blinded. For sheep red blood cell (SRBC) immunization, mice were injected intraperitoneally with SRBCs (Colorado Serum Company) once on day 0 and again on day 3. For FDC ablation, LT $\beta$ R-Fc and tumour necrosis factor receptor (TNFR)-Fc (100  $\mu$ g of each) or control IgG (provided by J. Browning) were injected intravenously and mice were analysed on day 4 after injection. Animals were housed in a pathogen-free environment in the Laboratory Animal Resource Center at the University of California, San Francisco, and all experiments conformed to ethical principles and guidelines that were approved by the Institutional Animal Care and Use Committee.

**Flow cytometry and cell sorting.** To identify human germinal-centre B cells and T<sub>FH</sub> cells, the following antibodies were used: fluorescein isothiocyanate (FITC)-conjugated anti-human CD4 (Tonbo, RPA-T4, 35-0049-T100); phycoerythrin (PE)-conjugated anti-human CXCR5 (ThermoFisher, MU5UBEE, 12-9185-41); PerCP-Cy5.5-conjugated anti-human CD38 (Biolegend, HIT2, 303518); PE-Cy7-conjugated anti-human CD19 (Biolegend, HIB19, 302216); allophycocyanin (APC)-conjugated anti-human IgD (Biolegend, IA6-2, 348221); and Pacific Blue-conjugated anti-human PD-1 (Biolegend, EH12.2H7, 329916). Cells were placed in a 96-well round bottom plate and washed with staining buffer (PBS containing 2% FBS, 0.1% sodium azide and 1 mM EDTA), and 25  $\mu$ l of antibody cocktail was added to each sample for 20 min on ice. After incubation, cells were washed twice with staining buffer. For staining of OX56, a 1:200 dilution of a biotinylated OX56 antibody was placed on the cells for 25 min on ice, after which the cells were washed and a 1:200 dilution of streptavidin-Alexa Fluor 647 (AF647) (Invitrogen) was incubated with the cells for 20 min. To identify Thy1.1 reporter expression, PE-conjugated anti-mouse/rat CD90.1 (Biolegend, OX-7) was used. For staining of pAKT or P2RY8, intracellular flow cytometry was performed on fixed cells (see details in 'pAKT stimulation, fixation and intracellular staining'). Data were acquired using a BD LSR II flow cytometer or a BD FACS Calibur. A BD FACSAria II was used to sort human tonsil subsets, and an example of the gating strategy and post-sort purity is provided in Extended Data Fig. 9a. Flow cytometry data were analysed using Flowjo (v.9.7.6).

**Generation of P2RY8-expressing WEHI-231 cells.** P2RY8 was cloned into the murine stem cell virus (MSCV)-GFP retroviral vector (P2RY8-GFP). The retrovirus encoding P2RY8-GFP was produced using the Platinum-E packaging cell line. Approximately  $5 \times 10^5$  WEHI-231 cells were placed in a 6-well plate along with the retroviral supernatant and the cells were centrifuged at 1,340g (2,400 r.p.m.) for 2 h at room temperature. The viral supernatant was aspirated and the cells were resuspended in growth medium and returned to culture. This spinfection was repeated with fresh retrovirus for a second time 24 h later. Then, 48 h after the second spinfection, the highest 5% of GFP-expressing cells were sorted using a BD FACSAria II. These cells were combined with GFP-negative cells in a 1:1 ratio and this mixture was maintained in culture for use in transwell bioassays.

**Migration inhibition transwell bioassay.** A confluent T25 flask containing a mixture of wild-type and P2RY8-GFP-transduced WEHI-231 cells was washed twice in pre-warmed migration medium (RPMI containing 0.5% fatty acid-free BSA, 10 mM HEPES and 50 IU penicillin/streptomycin). The cells were resuspended in migration medium at  $2 \times 10^6$  cells ml<sup>-1</sup> and resensitized for 10 min in a 37 °C water bath.

Recombinant human CXCL12 (Peprotech) was diluted to 50 ng ml<sup>-1</sup> in migration medium. Tissue extracts or purified compounds were diluted at varying concentrations in the CXCL12-containing migration medium, and 600  $\mu$ l of each of these mixtures was added to a 24-well tissue culture plate. Methanol-based extracts could be added to the medium at a concentration of up to 1:100 without interfering with overall WEHI-231 migration. In some experiments, 500 ng ml<sup>-1</sup> CXCL13 (Peprotech) was used instead of CXCL12. Transwell filters (6 mm insert, 5  $\mu$ m pore size, Corning) were placed on top of each well, and 100  $\mu$ l of P2RY8-GFP-expressing WEHI-231 cells ( $2 \times 10^5$  cells) was added to the transwell insert. The cells were allowed to migrate for 3 h, after which the cells in the bottom well were counted by flow cytometry. To assess migration inhibition, the proportion of P2RY8-GFP<sup>+</sup> cells that migrated for each well was divided by the proportion of P2RY8-GFP<sup>+</sup> cells that migrated to CXCL12 alone. This normalized metric is plotted as 'P2RY8<sup>+</sup> cells that migrate to CXCL12 (%)' for each bioassay. Representative experiments for each bioassay are also plotted as a percentage of input migration in Extended Data Fig. 9b. The baseline migration between experiments differs based on the growth state of the WEHI-231 cells.

**Cell lines and treatments.** HEK293T, HeLa, Hepa 1-6, MC38 and B16 cells were grown in 10-cm tissue culture dishes in DMEM containing 10% FBS, 10 mM HEPES, 2 mM glutamine and 50 IU penicillin/streptomycin. WEHI-231, Ly7,

Ly8, DOHH2 and M12 cells were grown in upright T25 flasks in RPMI containing 10% FBS, 10 mM HEPES, 2 mM glutamine, 55  $\mu$ M 2-mercaptoethanol and 50 IU penicillin/streptomycin. All cell lines were previously obtained from other laboratories and further authentication was not performed. The cell lines were not tested for mycoplasma contamination. For some experiments, DOHH2 cells were transduced with retrovirus encoding GNA13-IRES-GFP or empty vector-GFP.

To test bioactivity production, cells were plated out in either 12-well or 6-well plates and allowed to reach confluence. The medium was then replaced with serum-free medium (RPMI containing 0.5% fatty acid-free BSA, 10 mM HEPES and 50 IU penicillin/streptomycin) at 750  $\mu$ l per well for a 12-well plate or 1.5 ml per well for a 6-well plate; incubated for 16–18 h; and tested in the bioassay. Culturing cells in this serum-free media resulted in greater bioactivity production compared with culturing cells in media containing FBS. To test whether bioactivity production was dependent on albumin, the BSA in the serum-free media was titrated or removed entirely. The supernatant from these cultures was diluted 1:5 in migration assay media, mixed with CXCL12 and tested in the bioassay. For testing the effects of small-molecule inhibitors on bioactivity production, inhibitor-containing serum-free media were used to replace the growth media. After 16–18 h, the media were removed, centrifuged to remove cells and debris and tested at varying dilutions in the P2RY8 bioassay.

For transfection of HEK293T cells, mouse GGT1, GGT5, GGT6 and GGT7 and human GGT2 were cloned into an MSCV-Thy1.1 retroviral vector. HEK293T cells were seeded into 6-well tissue culture plates and grown until 75% confluent in antibiotic-free medium. To prepare the transfection mixture, the plasmids were aliquoted in Opti-MEM, then mixed with Lipofectamine 2000 (at 6  $\mu$ l per 3  $\mu$ g plasmid) and allowed to sit for 25 min at room temperature. The mixtures were gently added dropwise to the HEK293T cells. Then, 24 h after transfection, the medium was replaced with serum-free medium containing 1  $\mu$ M GGG or DMSO (vehicle control) for 18 h and the supernatants were tested in the bioassay. In some experiments, medium containing 10  $\mu$ M GGG was placed on transfected HEK293T cells for 7 h, after which the supernatant was purified for mass spectrometry analysis. Hepa 1-6 cells were retrovirally transduced with GGT5 and incubated with serum-free media containing 100 nM GGG or DMSO (vehicle control) for 18 h, and the supernatants were tested in the bioassay.

**Chemicals and reagents.** Indomethacin, ibuprofen, mevalonic acid, mevastatin, S1P and glutathione were purchased from Sigma. HPLC-grade solvents were purchased from Fisher. Leukotriene C<sub>4</sub>, leukotriene D<sub>4</sub> and GG-PP were purchased from Cayman Chemical. LPI was purchased from Avanti Polar Lipids. ETYA and AACOCF<sub>3</sub> were purchased from Biomol. GGG was chemically synthesized using the protocol specified in 'Chemical synthesis'.

**Transwell migration assay on human tonsil cells.** Fresh human tonsil tissue was obtained through the UCSF Biospecimen Resources (BIOS) Program from donors undergoing tonsillectomies, and analysed within 4–6 h after surgery (tissue was stored on ice in RPMI medium). Informed consent was obtained by the BIOS program, which complied with all ethical and regulatory requirements and de-identified the samples upon collection. Tonsils were mashed through a metal mesh to form a cell suspension and washed in migration medium. Because of blood contamination during surgery, red blood cells were lysed and the suspension was washed twice in warm migration medium and resensitized at  $10^7$  cells ml<sup>-1</sup> in migration assay medium in a 37 °C water bath for 10 min. A titration of GGG or 100 nM S1P was prepared with 100 ng ml<sup>-1</sup> CXCL12, and the different mixtures were placed in the bottom wells of a 24-well plate. Approximately  $10^6$  cells were placed into 5- $\mu$ m transwell filters (Corning Costar) and allowed to migrate for 1.5 h at 37 °C. Migrated cells were stained with antibodies against germinal-centre B cell and T<sub>FH</sub> cell markers and counted by flow cytometry.

**Purification of P2RY8 ligand from pig bile.** Frozen pig bile (60 ml), which was purchased from Pel-Freez Biologicals, was thawed in a 37 °C water bath. Saturated ammonium sulfate (SAS; pH 7.4) was added to the pig bile to achieve a 70% SAS solution, resulting in a large amount of precipitate. This was centrifuged for 15 min at 8,300g. The liquid was decanted and the precipitate was mixed thoroughly with 20 ml water. Methanol (120 ml) was added and the mixture was vortexed vigorously, followed by centrifugation for 15 min at 8,300g. The supernatant was transferred into an Erlenmeyer flask. The pellet was washed with 40 ml methanol to extract residual lipids and centrifuged for 15 min at 8,300g, and the supernatant was combined into the Erlenmeyer flask. To perform a Folch extraction (8:4:3 chloroform:methanol:water), 320 ml chloroform was added to the flask, along with 100 ml water. The flask was vigorously shaken and the resulting aqueous and organic layers were allowed to separate overnight. The upper (aqueous) layer was transferred to a separate Erlenmeyer flask. An additional 200 ml 1:1 methanol:water was added to the bottom (chloroform) layer and the flask was vigorously shaken again to further extract polar compounds. The layers were allowed to separate for 1 h, after which the upper aqueous layer was combined with the previous aqueous layer. To further remove non-polar compounds from this aqueous layer, 100 ml chloroform was added to this aqueous layer, shaken and allowed to

separate. The aqueous layer was transferred to a 4-l Erlenmeyer flask. A total of 3 l water acidified with 27 ml 1 M HCl was added to the bile extract, which caused a yellow-green precipitate to form. The solution was then divided into 500-ml Nalgene bottles and centrifuged at 8,700g (7,000 r.p.m.) in an ultracentrifuge. The supernatant was decanted and the green, wax-like pellet was dissolved in 400 ml 50% methanol. This extract was bound to a 10-g C18 solid-phase extraction (SPE) column (Waters) using a vacuum manifold (Agilent). The column was washed with 50 ml 50% methanol, and then the compounds were eluted with 50 ml 100% methanol. The methanol was evaporated under compressed air to produce 600  $\mu$ l of a concentrated extract with potent bioactivity on P2RY8-transduced cells.

HPLC purification was performed using an Agilent 1220 Infinity HPLC coupled with an Agilent 1260 Infinity Fractionator. HPLC-grade solvents were purchased from Fisher. The maximum injection amount was 100  $\mu$ l. For purifying larger amounts of sample, the sample was injected and run multiple times per column and the corresponding fractions per minute were pooled. For each column, solvent A: 100% water + 0.1% formic acid; and solvent B: 100% methanol + 0.1% formic acid. Fractions were collected every minute, concentrated via evaporation and tested at a 1:100 dilution via bioassay. The bioactive fractions were pooled, concentrated and run on the next column.

First separation: Phenomenex Luna C18, 100- $\text{\AA}$  pore size, 250  $\times$  10.00 mm, 10- $\mu$ m particle size, part no. 00G-4094-N0. Flow rate: 2 ml min<sup>-1</sup>. 0–2 min, 50% B; 2–26.5 min, ramp to 95% B; 26.5–36.5 min, 95% B; 36.5–37 min, ramp to 50% B; 37–38 min, 50% B.

Second separation: Thermo BDS Hypersil C8, 150  $\times$  4.6 mm, 5- $\mu$ m particle size, part no. 28205-154630. Flow rate: 1 ml min<sup>-1</sup>. 0–2 min, 50% B; 2–10 min, ramp to 90% B; 10–20 min, 90% B; 20–20.5 min, ramp to 50% B; 20.5–22 min, 50% B.

Third separation: Phenomenex Synergi Polar-RP 80- $\text{\AA}$  pore size, 150  $\times$  4.6 mm, 4- $\mu$ m particle size, part no. 00F-4336-E0. Flow rate: 1 ml min<sup>-1</sup>. 0–4 min, 50% B; 4–12 min, ramp to 95% B; 12–23 min, 95% B; 23–23.5 min, ramp to 50% B; 23.5–25 min, 50% B.

Fourth separation: Thermo APS-2 Hypersil, 150  $\times$  4.6 mm, 5- $\mu$ m particle size, part no. 30705-154630. Flow rate: 1 ml min<sup>-1</sup>. 0–4 min, 50% B; 4–12 min, ramp to 95% B; 12–23 min, 95% B; 23–23.5 min, ramp to 50% B; 23.5–25 min, 50% B.

**Purification of P2RY8 ligand from cell-culture supernatants.** Hepa 1-6 cells were grown in 16 T175 flasks using DMEM containing 10% FBS, 10 mM HEPES, 2 mM glutamine and 50 IU penicillin/streptomycin. When cells were confluent, the medium was replaced with RPMI containing 0.5% fatty acid-free BSA, 10 mM HEPES, 50 IU penicillin/streptomycin and 50  $\mu$ M nicardipine, a drug that we found increased bioactivity production specifically in Hepa 1-6 cells. To half of the flasks, 10  $\mu$ M mevastatin was also added to inhibit bioactivity production. After 24 h, the supernatant from each condition was collected from the cells and centrifuged at 800g (2,000 r.p.m.) to remove cell debris. Methanol was added to form a 20% methanol solution, and the solution was acidified to pH 3.5 using 1 M HCl. For each condition, the solution was bound to a 10-g C18 SPE column using a vacuum manifold. The columns were washed with 50 ml 50% methanol, and the compounds were eluted with 50 ml 100% methanol and then evaporated to produce 600  $\mu$ l of a concentrated extract. The extracts from statin-treated and control Hepa 1-6 cells were then simultaneously purified using the same HPLC and solvent system as for bile, using the Thermo BDS Hypersil C8, Phenomenex Synergi Polar-RP and Thermo APS-2 Hypersil columns. Fractions were collected every minute, concentrated via evaporation and tested at a 1:100 dilution via bioassay. The bioactive fractions for the control Hepa 1-6 cells were pooled, concentrated and run on the next column. The corresponding fractions from the statin-treated Hepa 1-6 cells were also pooled, concentrated and run simultaneously.

**SPE.** C18 SPE columns were purchased from Waters (Sep-Pak, 10 g 35 cc and 500 mg 6 cc versions). The SPE columns were attached to a vacuum manifold (Vac Elut 20, Agilent) and pressure was maintained at 13.8–34.5 kPa (2–5 psi). The column was washed with two column-volumes of methanol, then two volumes of water. Samples were typically diluted to a methanol content of 20% or lower, acidified to pH 3.5 and loaded onto the column at a drop rate of 1–2 drops per second. The column was washed with 2 volumes of water and 1 volume of 50% methanol. The compounds were then eluted with 1 volume of 100% methanol into glass test tubes. The solution was dried down using a Thermo Reacti-Vap apparatus under compressed air and the residue was dissolved in a small amount of 100% methanol. **Mass spectrometry.** An AB SCIEX QTRAP 6500 mass spectrometer was used to obtain full mass spectra (Q1), MS/MS fragment ion spectra and precursor ion spectra. HPLC fractions were diluted 1:10 in HPLC-grade methanol without any additives. The diluted samples were directly injected into the ion source via syringe at 10  $\mu$ l min<sup>-1</sup> and ionized using electrospray ionization (ESI). Mass spectra were acquired in both positive-ion and negative-ion mode. The ion source was maintained at 100  $^{\circ}$ C, 20 CUR, 14 GS1 and 8 GS2, 5,500 IS (positive mode) or –4,500 IS (negative mode), 135 DP (positive mode) or –60 DP (negative mode), EP 10 and CXP 10. A range of collision energy was used when performing fragmentation analysis. Positive- and negative-mode fragmentation spectra (MS/MS)

were obtained for the candidate ion. The mass of each fragment ion in the MS/MS spectra was input into Google to search for publications that reported molecules with similar fragmentation patterns. A study that contained the MS/MS spectra of glutathione was found<sup>7</sup>, and the glutathione spectra displayed many of the fragments observed in the MS/MS spectra of the candidate ion, suggesting the presence of similar chemical structures. Precursor ion scans in positive-ion mode using *m/z* 179 were used to detect Cys-Gly conjugates. The data were analysed using Analyst software.

To quantify GGG in tissues, an LC-MS/MS method was developed using synthetic GGG as a reference standard. GGG was detected using multiple reaction monitoring scans with ion pair 580.3 and 179.0, and GG-Cys-Gly was detected using ion pair 451.3 and 162.0. A reference standard for GG-Cys-Gly was produced by purifying supernatants from GGT5-expressing HEK293T cells incubated with GGG. Three microlitres of each sample was injected into a Shimadzu Nexera X2 HPLC, with a Synergi Polar-RP column (75  $\times$  4.6 mm) and a mobile phase gradient consisting of A: 100% H<sub>2</sub>O + 0.1% formic acid; and B: 100% acetonitrile + 0.1% formic acid. 0–1 min, 50% B; 1–4 min, ramp to 80% B; 4–6 min, 80% B; 6–6.5 min, ramp to 50% B; 6.5–8 min, 40% B. The internal standard used was LTC<sub>4</sub>-d<sub>5</sub>, identified with ion pair 631.4/179.0. Peak area was integrated using Analyst software and referenced against a standard curve to calculate compound abundance.

High-resolution LC-MS was performed using a Waters XEVO-G2 XS quadrupole time-of-flight with an Acquity UPLC equipped with a BEH C18 column. The mobile phase was H<sub>2</sub>O with 0.05% formic acid (A) and acetonitrile with 0.05% formic acid (B). 0.1–1.9 min, 5–95% B; 1.9–2.2 min, 95% B; 2.2–2.3 min, ramp down to 5% B; 2.3–2.6 min, 5% B. Mass spectra were acquired using ESI in positive-ion mode. Metabolite databases including the human metabolome database (HMDB), LipidMaps, LipidBank and Chempidder were used to search for the identity of the *m/z* 580.3435 candidate ion, although each query led to 0 matches.

**Chemical synthesis.** Unless otherwise noted, all materials used in chemical synthesis were obtained commercially from MilliporeSigma and were reagent grade. Nuclear magnetic resonance (NMR) spectra were obtained on a Bruker Avance III HD 400 MHz spectrometer.

For geranylgeranyl bromide, the previously outlined procedure<sup>24</sup> was followed. Triphenylphosphine (21.2 mg, 80.8  $\mu$ mol, 1.3 eq.) was added to a solution of geranylgeraniol (20 mg, 68.9  $\mu$ mol, 1 eq.) in 1 ml dry dichloromethane (DCM), stirring at room temperature under an atmosphere of argon. Carbon tetrabromide (29.6 mg, 89.3  $\mu$ mol, 1.3 eq.) was then added, and the reaction was stirred at room temperature for 4 h. The reaction mixture was concentrated under reduced pressure and a small volume of *n*-hexane was added. The resulting precipitate was removed by filtration and the filtrate was concentrated again under reduced pressure. The unstable product was used in the next step without further purification.

For GGG, a modified version of the previously described procedure<sup>25</sup> was used. L-glutathione (23.0 mg, 74.9  $\mu$ mol, 1.1 eq.) was dissolved in 0.5 ml 2 M NaOH, and approximately 1 ml ethanol was added drop-wise until the solution started to become cloudy. Geranylgeranyl bromide (24.0 mg, 68.7  $\mu$ mol, 1 eq.) was added drop-wise, and the reaction was stirred at room temperature overnight. The pH was then adjusted to 2 by addition of 1 M HCl and the mixture was cooled in an ice bath for 20 min. The resulting precipitate was collected by filtration, washed with ice-cold ethanol and water and dried to yield geranylgeranyl glutathione as an off-white solid (6.0 mg, 10.4  $\mu$ mol, 15%).

<sup>1</sup>H NMR ( $\delta$  p.p.m., DMSO-*d*<sub>6</sub>): 8.65 (1H, app. s, NH); 8.36 (1H, d, *J* = 8.17 Hz, NH); 5.20–5.14 (1H, m, CH); 5.12–5.04 (3H, m, CH); 4.48–4.39 (1H, m); 3.70 (3H, m); 3.32 (1H, m); 3.15 (3H, m); 2.89–2.80 (1H, m); 2.61–2.52 (1H, m); 2.42–2.22 (2H, m, CH); 2.10–1.90 (12H, m, 6  $\times$  CH<sub>2</sub>); 1.64 (3H, s, CH<sub>3</sub>); 1.63 (3H, s, CH<sub>3</sub>); 1.56 (9H, s, 3  $\times$  CH<sub>3</sub>).

ESI high-resolution MS (*m/z*): Calculated for chemical formula C<sub>30</sub>H<sub>49</sub>N<sub>3</sub>O<sub>6</sub>S [M + H]<sup>+</sup>, 580.3415; found 580.3435.

**Crude tissue-extract preparation.** Crude tissue extracts were prepared by grinding mouse tissues into water (1:10 w/v), then diluting this lysate with four volumes of methanol. The mixture was centrifuged twice at 4,000g for 5 min to remove precipitate. The supernatant was evaporated and the residue was dissolved in a small amount of 100% methanol. Raw mouse bile was collected directly from the gallbladder using a syringe.

To obtain C18 solid-phase extracts of spleen, lymph nodes and tonsil, tissue was homogenized in 66% methanol using a Precellys 24-bead homogenizer, 1:10 w/v. For mass spectrometry analysis, 20–100 mg of tissue was homogenized along with 15  $\mu$ l of a 150 nM solution of LTC<sub>4</sub>-d<sub>5</sub> as an internal standard. The homogenate was transferred to a new tube. Then, 500  $\mu$ l 66% methanol was used to wash the beads and was combined with the homogenate. The mixture was centrifuged for 10 min at 4,000g in a microcentrifuge and the supernatant was diluted tenfold in water containing 3 mM HCl. This was then bound to a 500-mg C18 SPE column, washed with 50% methanol, eluted with 100% methanol and concentrated down to 100  $\mu$ l by evaporation.

**Size-exclusion centrifugal filtration of bile and cell-culture supernatant.** Amicon centrifugal filtration units with 50-kDa-cutoff membranes were used

purchased from Millipore. A 100-fold dilution of raw mouse bile in RPMI or undiluted HEK293T culture supernatant (serum-starved, 0.5% BSA) was loaded into the top chamber of each type of centrifugal filtration unit. The unit was centrifuged at 7,500g for 15 min in a fixed-angle rotor. The filtrate in the bottom chamber of the filtration unit and the concentrate in the upper chamber of the filtration unit were tested for P2RY8 bioactivity.

**Internalization assay.** P2RY8, GPR55, S1PR2, CYSLTR1 and CYSLTR2 were cloned into an MSCV-Thy1.1 retroviral vector with an OX56 (rat CD43-derived<sup>26</sup>) epitope tag to track surface expression levels of each receptor using the OX56 antibody. P2RY8-OX56-Thy1.1 was retrovirally transduced into M12 cells, and the other G-protein-coupled receptor constructs were transduced into WEHI-231 cells. Confluent cultures of each of the lines indicated above were washed twice in migration medium, resuspended at  $5 \times 10^6$  cells ml<sup>-1</sup> and resensitized at 37 °C for 10 min. For each line, 20 µl of cells was aliquoted into a 96-well plate. GGG, LPI, S1P, LTC<sub>4</sub> and LTD<sub>4</sub> were prepared in migration medium and 80-µl aliquots were placed into a 96-well round bottom plate such that the concentration after adding the cells would be as indicated in the figures. Using a multichannel pipette, the compounds were placed on the cells, and the plate was placed in a 37 °C cell culture incubator for 45 min. The plate was then placed on ice, washed with ice-cold flow cytometry buffer and stained for OX56 levels by flow cytometry. OX56 surface levels on transduced cells were assessed by drawing a gate on the top 40% of OX56-expressing cells in the control condition, then using the same gate on the transduced cells treated with various compounds to assess internalization.

**pAKT stimulation, fixation and intracellular staining.** DLBCL lines, P2RY8-GFP WEHI-231 cells or human tonsil cells were washed twice in migration medium and resensitized for 10 min at 37 °C. In 5-ml polystyrene FACS tubes,  $5 \times 10^4$  cells were diluted in 500 µl of migration medium containing the indicated combinations of 100 ng ml<sup>-1</sup> CXCL12, 100 nM GGG, 100 nM S1P and 200 nM wortmannin, for either 10 min (human tonsil cells) or 5 min (DLBCL lines, WEHI-231 cells). Afterwards, 50 µl 16% paraformaldehyde (PFA) was added to each tube. The cells were fixed at room temperature for 10 min and centrifuged, and 1 ml cold methanol was added to each tube while vortexing. The samples were placed at -20 °C overnight, washed three times with FACS buffer, blocked for 20 min at room temperature with 5% normal goat serum (Sigma) and 1:100 Fc-block, stained at room temperature for 1 h with a 1:100 dilution of rabbit anti-pAKT (Cell Signaling Technology, Ser473, clone D9E), washed twice in FACS buffer and stained for 1 h at room temperature with a 1:300 dilution of APC-conjugated goat anti-rabbit-IgG (Santa Cruz Biotechnologies), or AF647-conjugated goat anti-rabbit IgG (Invitrogen) in some experiments. It was noted that unstimulated P2RY8<sup>+</sup> WEHI-231 cells had a lower pAKT level, which might reflect endogenous production of small amounts of GGG. For human tonsil cells, antibodies towards germinal-centre B cell markers were added alongside the APC-conjugated goat anti-rabbit-IgG, and PE-conjugated anti-human IgD was used instead of APC-conjugated anti-human IgD. For staining of P2RY8 in DLBCL lines or human tonsil cells, the cells were fixed, permeabilized, blocked and stained as above, using a rabbit polyclonal anti-P2RY8 antibody (Sigma-Atlas Antibodies, HPA003631) that targets the intracellular C terminus of P2RY8, and an AF647-conjugated goat anti-rabbit-IgG antibody (Invitrogen).

**CRISPR-Cas9 targeting of P2RY8 in Ly8 cells.** The lentiCRISPR v2 system (purchased from Addgene) was used to disrupt P2RY8 in Ly8 cells. A non-targeting control guide (GAGATGATAACTTAATTTGT) or a guide targeting P2RY8 (GATCATGAAGATGACCGACG) was cloned into the lentiCRISPR v2 plasmid. Lentivirus for each construct was produced in HEK293T cells and Ly8 cells were spininfected for 2 h at room temperature. The infected Ly8 cells were allowed to recover for two days, after which the transduced cells were selected using puromycin (5 µg ml<sup>-1</sup>, Invivogen) for two weeks. Targeting of P2RY8 was assessed by extracting genomic DNA from the culture and performing TIDE analysis<sup>27</sup> on a PCR product encompassing the expected cut-site, which indicated an editing efficiency of 83% (<https://tide.deskgen.com/>). P2RY8 protein levels were also assessed using flow cytometry.

**Adoptive co-transfer of transduced B cells.** EasySep kits were used to enrich B cells from mouse spleens by removing T cells with biotin-conjugated anti-CD3ε (Biolegend, clone 145-2C11) and streptavidin-conjugated beads (EasySep Streptavidin RapidSpheres). B cells were cultured in 6-well plates with a final concentration of 0.25 µg ml<sup>-1</sup> (1:4,000 dilution) anti-CD180 (BD Biosciences, clone RP/14), diluted in RPMI 1640 containing 10% FBS, 10 mM HEPES, 55 µM 2-mercaptoethanol, 2 mM glutamine and 50 IU penicillin/streptomycin. Twenty-four hours after activation, the plate was centrifuged and the culture supernatant was saved. Retrovirus encoding MSCV-P2RY8-GFP, MSCV-EV-GFP, MSCV-EV-Thy1.1 or MSCV-GGT5-Thy1.1 was produced using the Platinum-E packaging cell line and added to separate plates of activated B cells. The B cells were spininfected at 2,400 r.p.m. for 2 h at room temperature, the viral supernatant was aspirated and the original culture supernatant was returned to the cells. This spininfection was repeated for a second time, 24 h later. Twenty-four hours after the second

spininfection, cells were collected from each plate and washed twice. qPCR analysis established that S1PR2 was not upregulated on the transduced cells. Approximately  $2 \times 10^7 - 3 \times 10^7$  P2RY8-GFP or empty vector-GFP B cells were mixed with  $4 \times 10^7 - 5 \times 10^7$  empty vector-Thy1.1 B cells or GGT5-Thy1.1 B cells, and adoptively transferred into unimmunized *Cd19*<sup>-/-</sup> mice (which lack germinal centres) on day 6 after immunization with SRBCs. Mice were analysed 24 h after transfer. Transduced cells comprised 1–3% (GFP) or 3–5% (Thy1.1) of all B cells in the spleen by flow cytometry. Positioning of GFP-expressing and Thy1.1-expressing B cells was tracked by immunofluorescence.

**RNAscope in situ hybridization.** RNA in situ hybridization was performed using the RNAscope RED 2.5HD manual assay kit (Advanced Cell Diagnostics) The RNAscope probe used for mouse GGT5 targeted region 996–2,040 of NM\_011820.5. Tissues were frozen in optimal cutting temperature compound (OCT). Within 1 h, 10-µm cryosections were cut and slides were dried at -20 °C for 20 min. Serial sections for each slide were stored at -20 °C for immunohistochemistry analysis of FDCs. Slides were fixed for 15 min with ice-cold 4% paraformaldehyde and washed in 50%, 70% and 100% ethanol for 5 min each. After drying for 5 min, slides were treated with hydrogen peroxide (from kit) for 8 min and protease IV (from kit) for 12 min. Probes were allowed to hybridize in a HybEZ oven at 40 °C for 3.5 h. The following incubation times for the amplification steps were used: Amp 1, 35 min; Amp 2, 20 min; Amp 3, 35 min; Amp 4, 20 min; Amp 5, 40 min; Amp 6, 25 min. Slides were then developed with FastRed (from kit) for 15 min, washed in PBS and counterstained for IgD using goat anti-mouse IgD (Cedarlane Laboratories) and horseradish peroxidase (HRP)-conjugated donkey anti-goat IgG (Jackson Immunoresearch).

**Immunohistochemistry and immunofluorescence.** Pieces of human tonsil tissue were fixed in 4% PFA for 2 h at 4 °C, washed with PBS, submerged in 30% sucrose overnight and embedded in OCT. For staining human GGT5 and CD21, cryosections of 7 µm were dried for 1 h at room temperature and then subjected to heat-induced antigen retrieval (HIER) by placing the slide in a solution of 1 × RNAscope target retrieval reagent (cat. no. 322000) at 95 °C for 1 h. Slides were allowed to cool for 20 min, then placed in ddH<sub>2</sub>O at room temperature for 10 min and blocked in TBS containing 0.1% fatty acid-free BSA for 10 min. A 1:200 dilution of rabbit anti-human GGT5 (Thermo, PA5-52514) or biotin-conjugated anti-human CD21 (Biolegend, clone Bu32, 354913) along with 1% NMS and NDS (Sigma) was incubated with the slides for 2 h at room temperature. The slides were washed, and a 1:200 dilution of HRP-conjugated anti-rabbit-IgG or HRP-conjugated streptavidin (Jackson Immunoresearch) was incubated with the slides for 2 h at room temperature. The slides were developed using Sigma DAB and counterstained with haematoxylin. For immunofluorescence, a 1:200 dilution of AF647-conjugated goat anti-rabbit-IgG (Invitrogen), streptavidin-conjugated AF555 (Invitrogen) or Cy3 (Jackson Immunoresearch) and DAPI was used to visualize the co-localization of GGT5 and CD21 signals. For staining human P2RY8, cryosections were stained with a 1:200 dilution of rabbit anti-human P2RY8 (Sigma-Atlas Antibodies, HPA003631). In some experiments, non-HIER-treated sections were co-stained with anti-human P2RY8 and biotin-conjugated anti-human CD4 (Biolegend, clone RPA-T4), because the CD4 epitope was degraded by heat treatment. The same secondary antibodies as above were used. The GGT5 stain required HIER, but the P2RY8 stain produced similar results with or without HIER.

To track the positioning of GFP- or Thy1.1-expressing B cells, mouse tissues were fixed in 4% PFA for 2 h at 4 °C, washed with PBS, submerged in 30% sucrose overnight and embedded in OCT. Cryosections of 7 µm were dried for 1 h at room temperature and rehydrated in PBS containing 0.1% fatty acid-free BSA for 10 min. A 1:100 dilution of biotin-conjugated anti-Thy1.1 (eBioscience) or AF488-conjugated rabbit anti-GFP (Invitrogen) was used. For immunized mice, biotin-conjugated anti-mouse CD35 was used to track FDC positioning. Endogenous naive B cells were labelled using goat anti-mouse IgD (Cedarlane Laboratories, GAM/IGD(FC)/7S). Antibodies were diluted with 1% NMS and NDS and incubated with the slides overnight at 4 °C. The slides were then washed in PBS and stained with AF647-conjugated streptavidin and AMCA-conjugated donkey anti-goat IgG for 2 h at room temperature, and images were captured with a Zeiss AxioObserver Z1 inverted microscope.

For analysis of CR1 (CD35) staining in serial sections from RNAscope tissues, the serial sections that were stored at -20 °C were fixed in cold acetone for 10 min and dried at room temperature for 1 h. Slides were rehydrated for 10 min in TBS containing 0.1% fatty acid-free BSA. A 1:100 dilution of biotin-conjugated anti-mouse CD35 (8C12, BD Biosciences) or goat anti-mouse IgD, with 1% NMS and NDS, was incubated with the slides overnight at 4 °C. The slides were washed in TBS and stained with alkaline phosphatase-conjugated streptavidin and HRP-conjugated donkey anti-goat IgG (1:100 dilution, Jackson Immunoresearch) for 2 h at room temperature. Slides were washed and sequentially developed using Sigma DAB and Fast Blue (Sigma).

**Image quantification.** Immunofluorescence images were imported into IMARIS software (v.7.4.2). Using the 'spots' function, single B cell follicles were chosen

as the region of interest and GFP<sup>+</sup> cells within these follicles were automatically labelled by the software. The centre of the follicle was marked using the 'measurement points' function. The distance of each labelled cell from the measurement point at the centre of the follicle was calculated, and used to determine the average distance of GFP<sup>+</sup> cells from the centre of the follicle. Three or four similarly sized follicles from each biological replicate were chosen randomly and quantified for each condition tested.

**Quantitative PCR.** Total RNA from tissues or sorted cells was extracted using an RNeasy kit (Qiagen) and reverse-transcribed using M-MLV reverse transcriptase. Tonsil and spleen stroma was prepared by gently mashing the tissue in a 70- $\mu$ m cell strainer and using saline to wash away the lymphocytes. The tissue aggregates remaining in the strainer, which are enriched in stromal cells, were extracted for qPCR analysis. qPCR was performed using Power SYBR Green with an Applied Biosystems StepOnePlus instrument. Data were analysed with the comparative C<sub>t</sub> ( $2^{-\Delta\Delta C_t}$ ) method, using the housekeeping genes indicated in the figures.

**Statistical analysis.** Prism software (GraphPad v.7.0e) was used for all statistical analyses. The statistical tests used are specified in the figure legends. Two-tailed unpaired *t*-tests were performed when comparing only two groups, and ordinary one-way ANOVA using Bonferroni's multiple comparisons test was performed when comparing one variable across multiple groups.  $P < 0.05$  was considered significant. In summary graphs, points indicate individual samples and horizontal

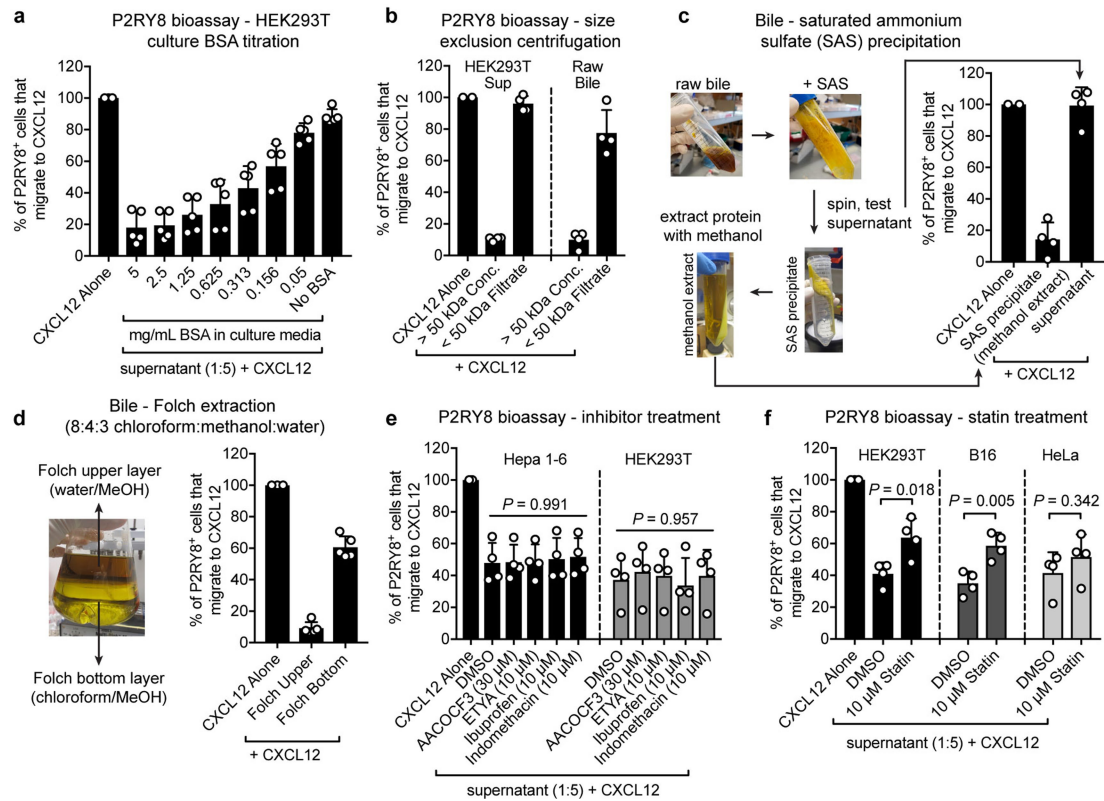
lines are means. In bar graphs, bars show means and error bars indicate standard deviation.

**Reporting summary.** Further information on research design is available in the Nature Research Reporting Summary linked to this paper.

### Data availability

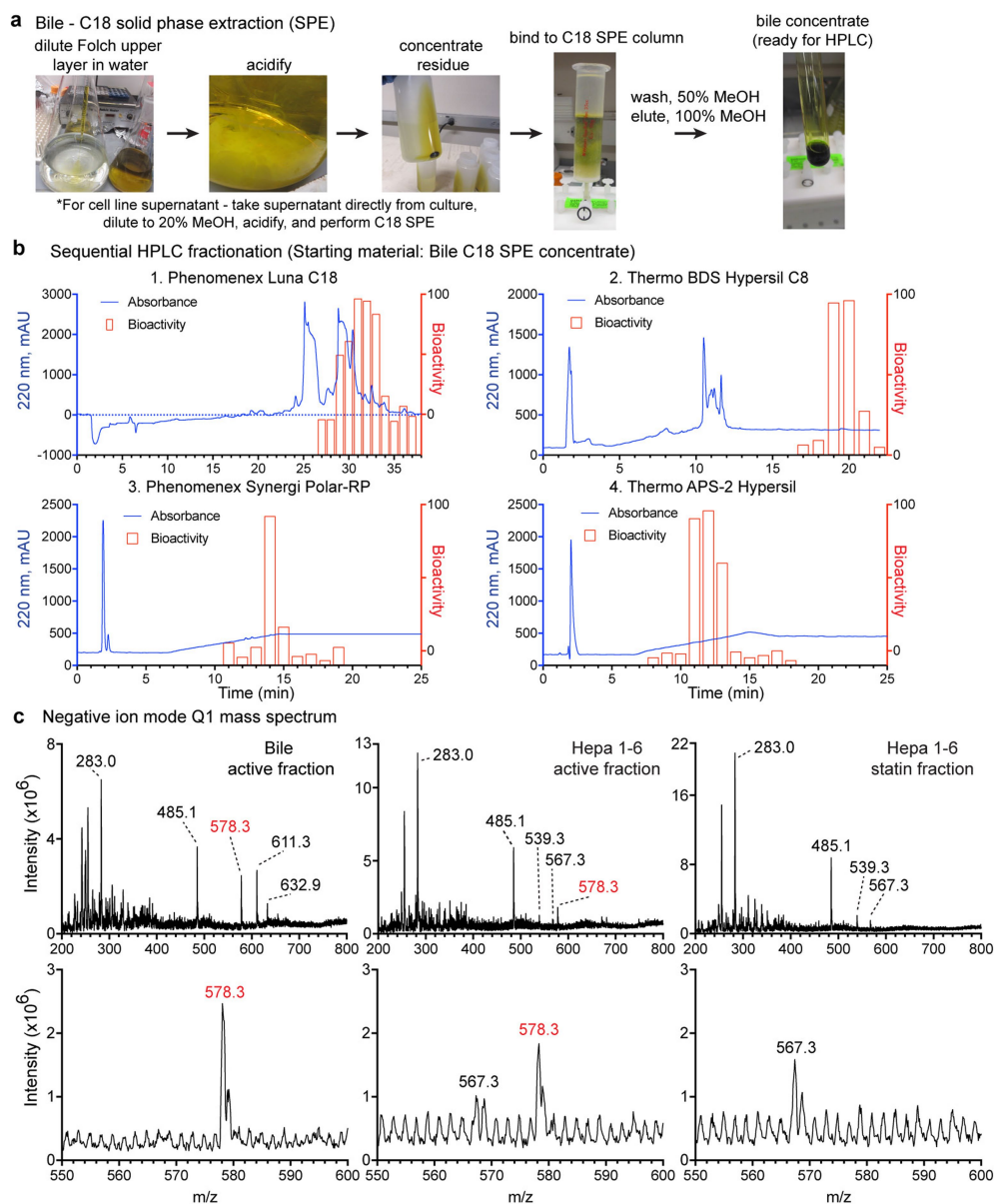
The data that support the findings of this study are available from the authors upon reasonable request. Source Data for experiments involving animal models or tonsil specimens are provided with the paper.

24. Liu, W., Zhang, Y., Hou, S. & Zhao, Z. K. Synthesis of isoprenoid chain-contained chemical probes for an investigation of molecular interactions by using quartz crystal microbalance. *Tetrahedr. Lett.* **54**, 6208–6210 (2013).
25. Niegowski, D. et al. Crystal structures of leukotriene C<sub>4</sub> synthase in complex with product analogs: implications for the enzyme mechanism. *J. Biol. Chem.* **289**, 5199–5207 (2014).
26. Cyster, J. G., Shotton, D. M. & Williams, A. F. The dimensions of the T lymphocyte glycoprotein leukosialin and identification of linear protein epitopes that can be modified by glycosylation. *EMBO J.* **10**, 893–902 (1991).
27. Brinkman, E. K., Chen, T., Amendola, M. & van Steensel, B. Easy quantitative assessment of genome editing by sequence trace decomposition. *Nucleic Acids Res.* **42**, e168 (2014).



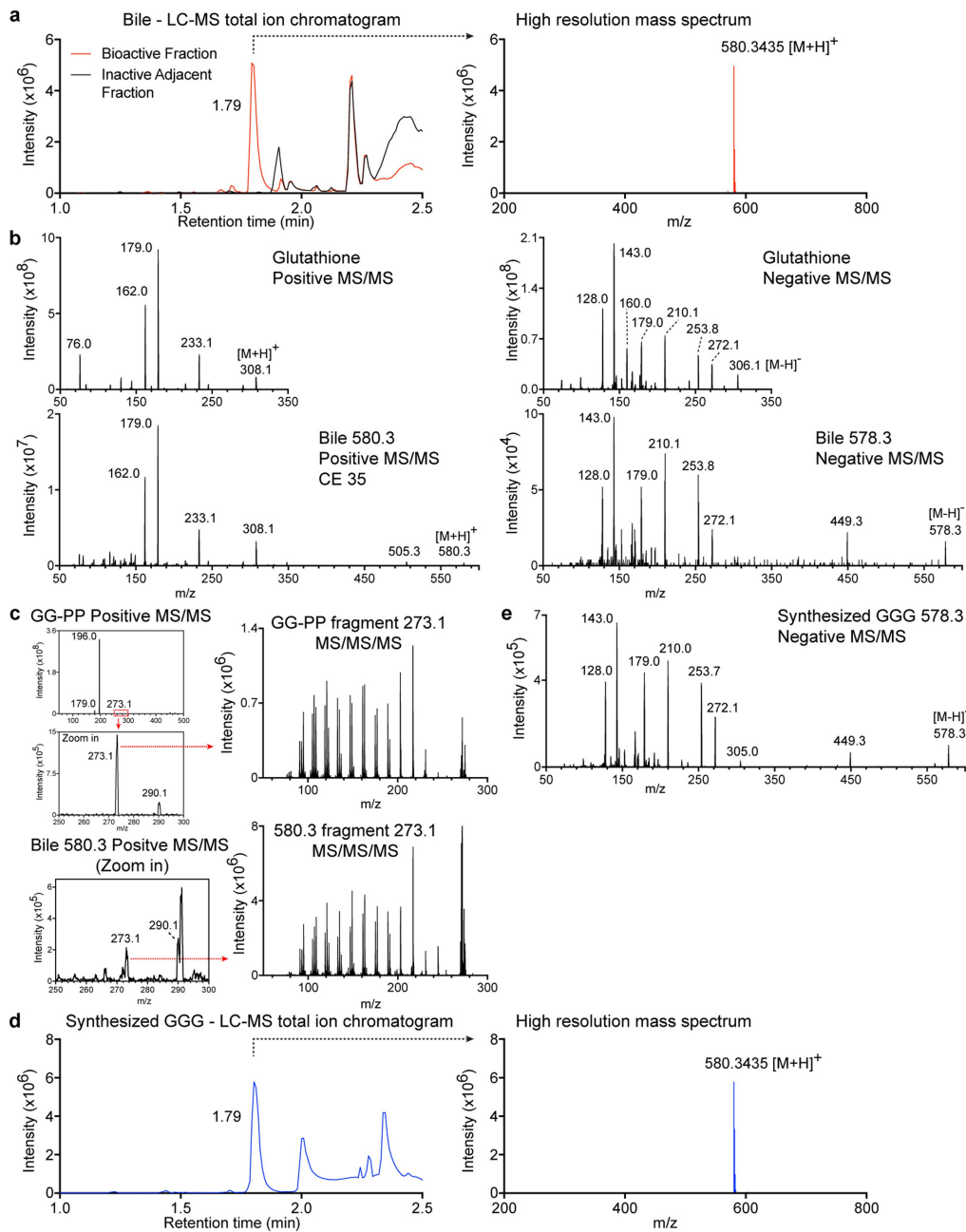
**Extended Data Fig. 1 | Dependence of P2RY8 bioactivity on albumin and the isoprenoid biosynthetic pathway.** **a**, Serum-free medium containing the indicated amounts of fatty acid-free BSA was placed on HEK293T cells for 16–18 h. The supernatants from these cultures were combined with CXCL12 in migration medium (1:5 dilution) and tested for P2RY8 bioactivity ( $n = 5$ ). **b**, P2RY8 ligand bioassay on 50 kDa concentrate (molecules >50 kDa) versus filtrate (molecules <50 kDa) from serum-starved HEK293T supernatant (left) or raw mouse bile (right) ( $n = 4$ ). **c**, Diagram of protein precipitation from pig bile using saturated ammonium sulfate (SAS) and methanol extraction of the SAS protein precipitate. Graph shows P2RY8 ligand bioassay of the SAS supernatant

and methanol extracts from the protein precipitate, as indicated by arrows ( $n = 4$ ). **d**, P2RY8 ligand bioassay of the two layers of a Folch extraction prepared by adding chloroform and water to the methanol extract of the SAS precipitate described in **c** ( $n = 5$ ). **e**, P2RY8 ligand bioassay on supernatants from Hepa 1-6 or HEK293T cells treated with the indicated inhibitors for 16 h ( $n = 4$ ,  $P$  values determined by one-way ANOVA). **f**, P2RY8 ligand bioassay on supernatants from HEK293T, HeLa or B16 cells treated with 10 μM mevastatin or vehicle (DMSO) for 16 h ( $n = 4$ ,  $P$  values determined by unpaired two-tailed  $t$ -test for the indicated comparisons). Data are pooled from three independent experiments (**a–f**). Graphs depict mean with s.d. and points represent biological replicates.



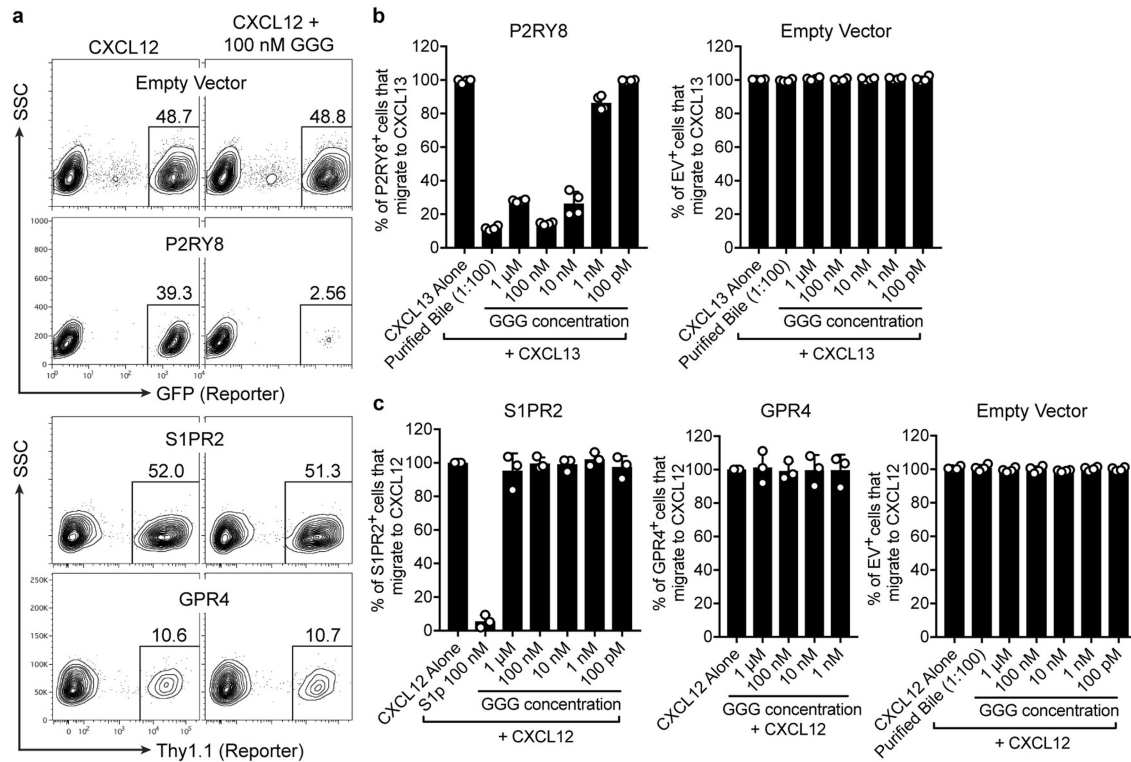
**Extended Data Fig. 2 | HPLC fractionation of P2RY8 bioactivity from bile and Q1 mass spectrometry candidate identification.** **a**, Preparation of a concentrated bile extract from the Folch upper layer described in Extended Data Fig. 1d using acid precipitation, centrifugation and C18 SPE. **b**, HPLC chromatograms (blue) showing absorbance at 220 nm for each column used for fractionation. Columns were initially tested with a small amount of extract to determine the interval in which bioactivity

eluted. The bioactivity graphs (red) that correspond to 1-min fractions are overlaid for the bioactive interval and represent the percentage of P2RY8<sup>+</sup> cells that are inhibited in their migration towards CXCL12 in the P2RY8 ligand bioassay. **c**, Full scan (Q1) mass spectra of purified fractions from the indicated conditions, in negative-ion mode. Zoomed-in spectra of *m/z* values of 550–600 are shown directly below each Q1 scan. Data are representative of two (**a**, **b**) or one (**c**) independent experiments.



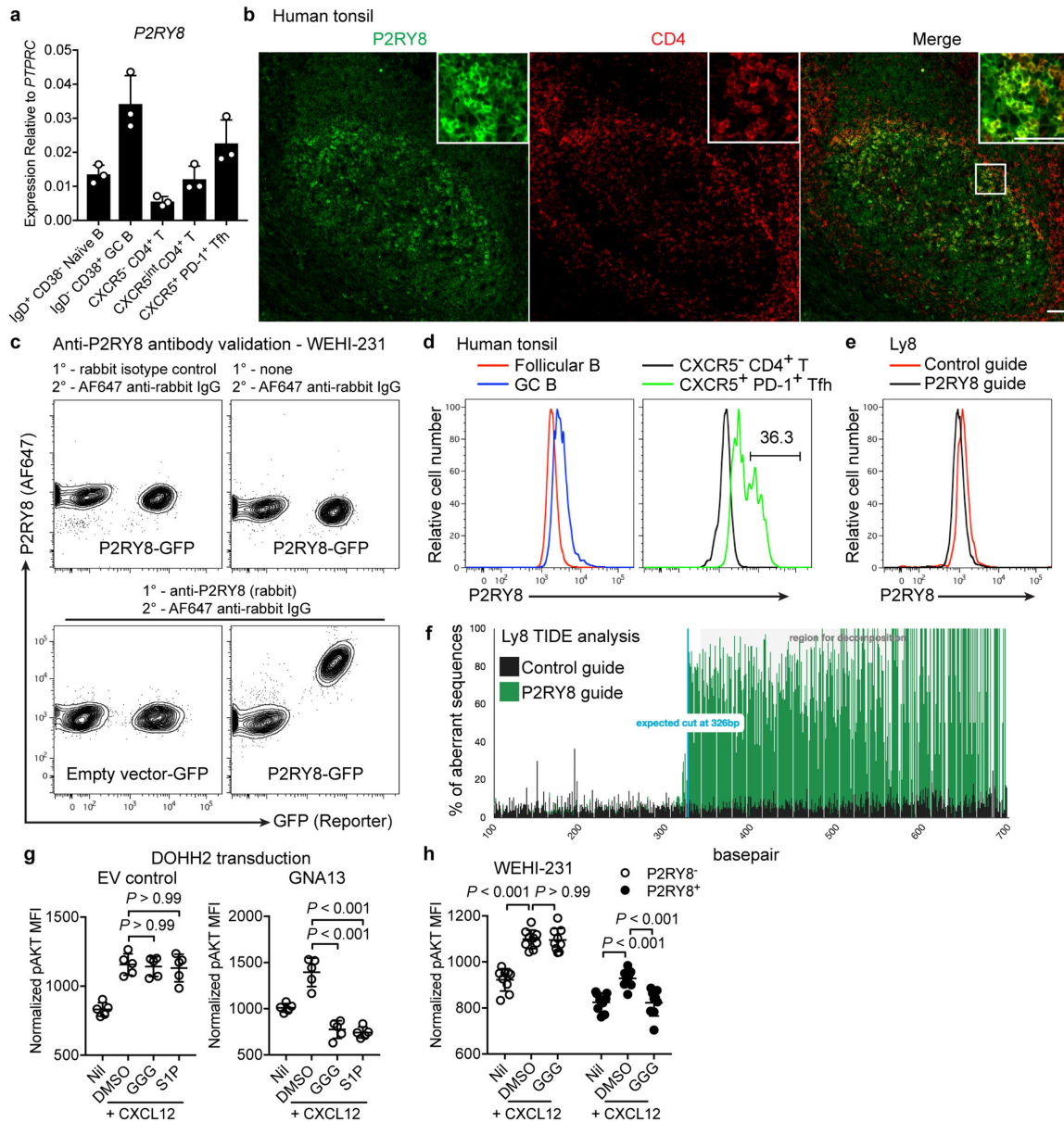
**Extended Data Fig. 3 | High-resolution mass spectrometry and fragmentation analysis suggest that the bioactive compound is a derivative of glutathione and geranylgeranyl.** **a**, Left, positive-ion mode LC-MS total-ion chromatogram of purified bile bioactive fraction (red), overlaid with an adjacent non-bioactive fraction (black). Right, high-resolution mass spectrum from time 1.79 of the active fraction. **b**, MS/MS fragmentation spectra of glutathione in positive-ion mode (top left) and negative-ion mode (top right), compared with MS/MS spectra of purified bile positive-ion 580.3 (bottom left) and negative-ion 578.3 (bottom right).

CE, collision energy. **c**, Positive-ion mode MS/MS/MS fragmentation spectra of the 273.1 ion present in the MS/MS spectra of GG-PP (top) and purified bile ion 580.3 (bottom; zoomed-in spectra from **b**). **d**, Positive-ion mode LC-MS total-ion chromatogram (left) and high-resolution mass spectra (right) from time 1.79 of chemically synthesized GGG. **e**, Negative-ion mode MS/MS spectra of the 578.3 ion from chemically synthesized GGG. Compare to the MS/MS spectra for the 578.3 ion from purified bile in **b**. Data are representative of two (**b**, **c**, **e**) or one (**a**, **d**) independent experiments.



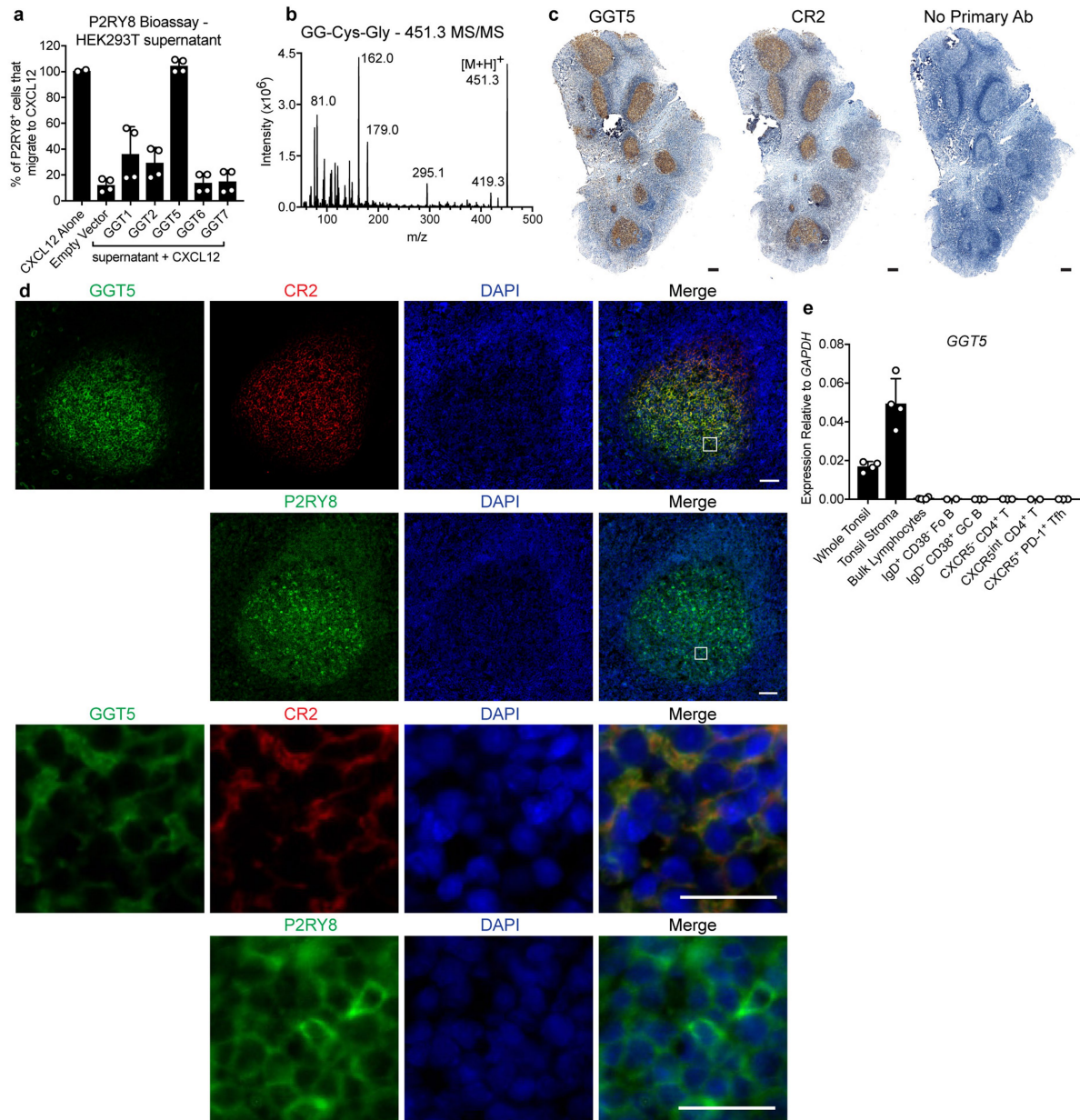
**Extended Data Fig. 4 | GGG specifically inhibits migration of P2RY8-expressing WEHI-231 cells.** **a**, Representative flow cytometry plots of migration-inhibition assays performed with  $50 \text{ ng ml}^{-1}$  CXCL12 and  $100 \text{ nM}$  GGG on WEHI-231 cells transduced with empty vector-GFP, P2RY8-GFP, S1PR2-Thy1.1 or GPR4-Thy1.1. **b**, Transwell migration-inhibition assay using  $500 \text{ ng ml}^{-1}$  CXCL13 and the indicated amounts of GGG for WEHI-231 cells transduced with P2RY8-GFP and empty

vector-GFP ( $n = 4$ ). **c**, Summarized data for WEHI-231 cells transduced with S1PR2-Thy1.1, GPR4-Thy1.1 and empty vector-GFP from assays of the type in **a** (S1PR2 and GPR4,  $n = 3$ ; empty vector,  $n = 4$ ). Data are representative of two independent experiments (**a**) and pooled from two independent experiments (**b**, **c**). Graphs depict mean with s.d. and points represent biological replicates.



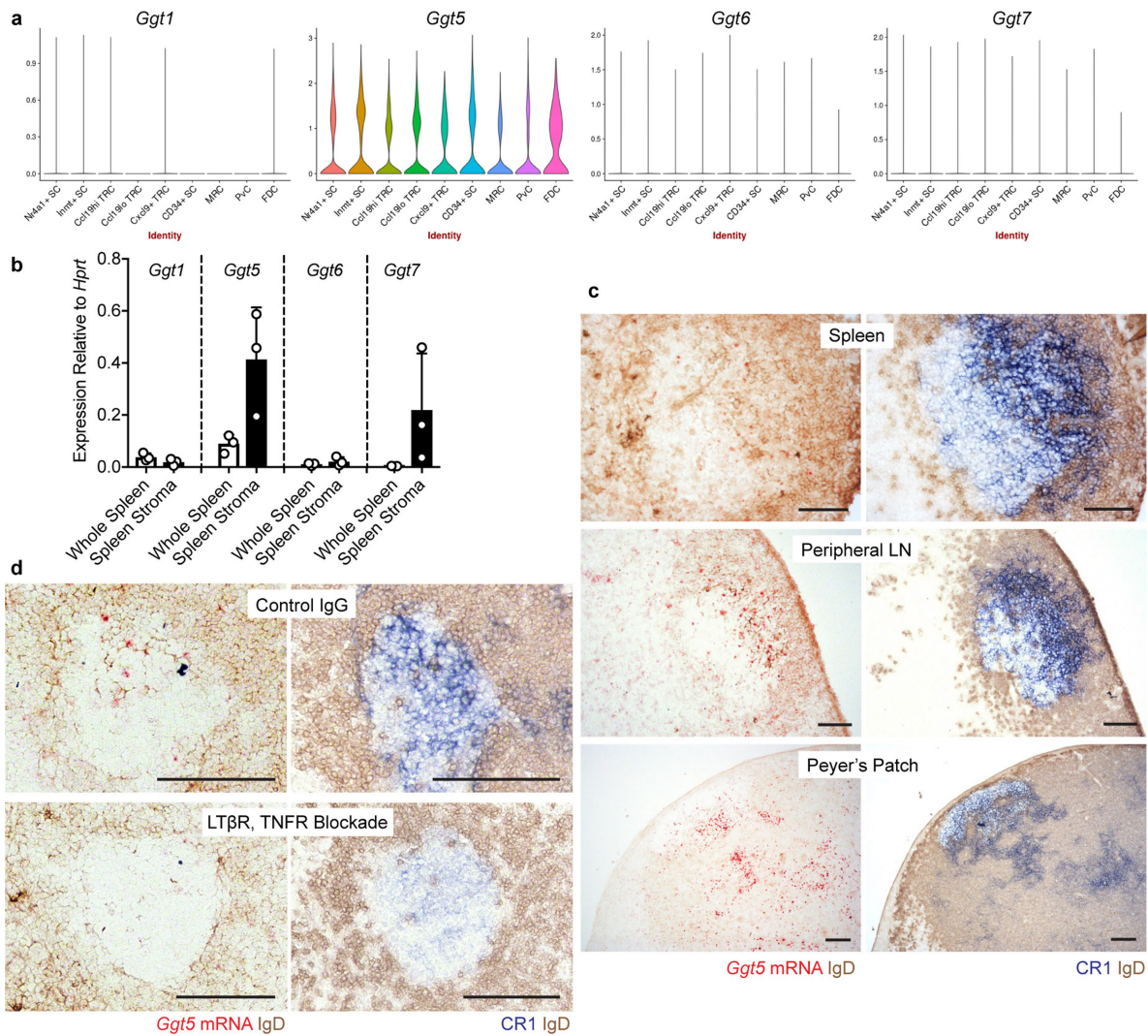
**Extended Data Fig. 5 | *P2RY8* expression and distribution in human tonsil.** **a**, qPCR for expression of *P2RY8* in the indicated subsets sorted from human tonsil, relative to *PTPRC*. ( $n = 3$ ) **b**, Immunofluorescence for *P2RY8* (green) and *CD4* (red) in PFA-fixed human tonsil sections. Inset depicts *P2RY8*<sup>+</sup> and *P2RY8*<sup>high</sup> expressing *CD4*<sup>+</sup> cells within the germinal centre and at the germinal-centre border. Scale bars, 50  $\mu\text{m}$ . **c**, Intracellular flow cytometry using the anti-*P2RY8* antibody from **b**, which binds the C terminus of *P2RY8*, on empty vector-GFP- or *P2RY8*-GFP-transduced WEHI-231 (mouse) cells, compared with rabbit isotype control or no primary antibody staining conditions. **d**, Intracellular flow cytometry for *P2RY8* in tonsil *IgD*<sup>+</sup> *CD38*<sup>-</sup> follicular B cells, *IgD*<sup>-</sup> *CD38*<sup>+</sup> germinal-centre B cells, *CXCR5*<sup>-</sup> *CD4*<sup>+</sup> T cells or *CXCR5*<sup>+</sup> *PD-1*<sup>+</sup> T<sub>FH</sub>

cells. **e**, Intracellular flow cytometry for *P2RY8* in Ly8 cells edited using CRISPR-Cas9 with a control non-targeting guide (red) or a guide targeting *P2RY8* (black). **f**, TIDE analysis of edited Ly8 cells showing editing efficiency around the expected cut site. **g**, pAKT levels in DOHH2 cells transduced with either GNA13 or empty vector, treated as in Fig. 3a ( $n = 5$ ). **h**, pAKT levels in *P2RY8*-expressing or control WEHI-231 cells, treated as indicated ( $n = 9$ ). Data are representative of or pooled from three (**a**), four (**b**) or two (**d**) tonsils; and four (**h**), two (**c**, **e**, **g**) or one (**f**) experiments. Graphs depict mean with s.d. Points represent biological replicates. *P* values determined by one-way ANOVA with Bonferroni's multiple comparisons test (**g**, **h**).



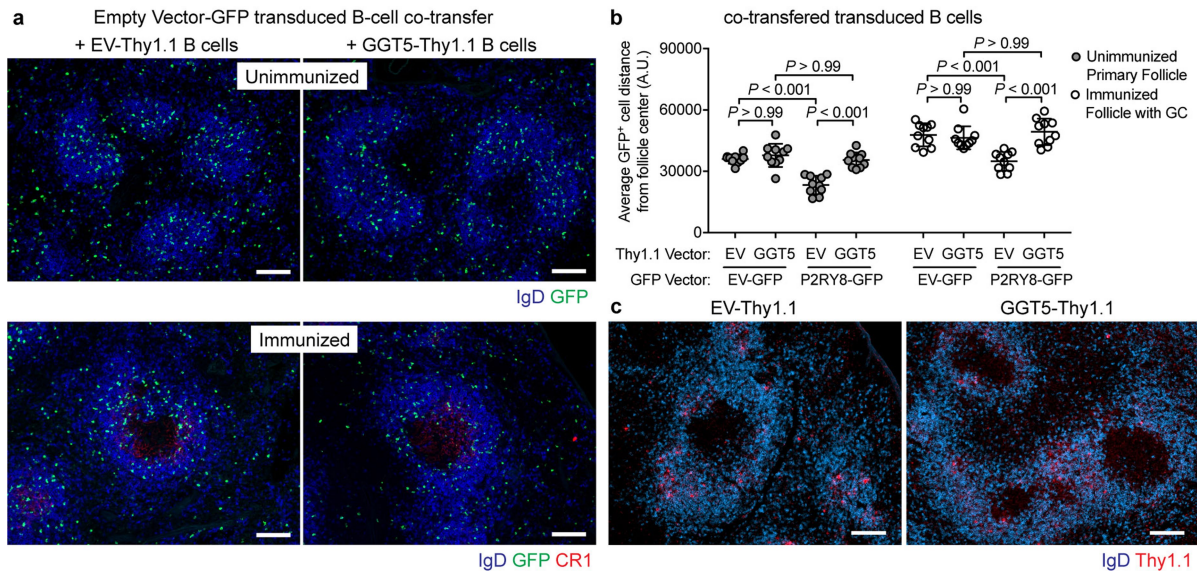
**Extended Data Fig. 6 | Expression of GGT5 by human tonsil FDCs and fragmentation pattern of S-geranylgeranyl-L-Cys-Gly.** **a**, P2RY8 ligand bioassay on supernatants from HEK293T cells transfected with the indicated enzymes ( $n = 4$  biological replicates). **b**, Positive-ion mode MS/MS spectra of the  $m/z$  451.3 metabolite from extracts of the type in Fig. 4d, corresponding to S-geranylgeranyl-L-Cys-Gly. **c**, Immunohistochemistry for GGT5 or CR2 (brown), in serial sections of human tonsil, counterstained with haematoxylin (blue). Ab, antibody. Scale bars, 200  $\mu\text{m}$ . **d**, Immunofluorescence for GGT5 (green), CR2 (red) and DAPI (blue) in tonsil sections. Serial sections were stained for P2RY8 (green) and DAPI (blue) to visualize the difference between FDC extensions

and germinal-centre B cell membranes. The indicated regions in the top panels (scale bars, 100  $\mu\text{m}$ ) are enlarged in the bottom panels (scale bars, 25  $\mu\text{m}$ ). **e**, qPCR for GGT5 expression in the indicated tissues and cells from human tonsil, relative to GAPDH. Points within each category represent individual tonsils (whole tonsil,  $n = 4$ ; tonsil stroma,  $n = 4$ ; bulk lymphocytes,  $n = 4$ ; follicular B cells (Fo B),  $n = 2$ ; germinal-centre B cells (GC B),  $n = 3$ ; CXCR5<sup>-</sup>CD4<sup>+</sup> T cells,  $n = 3$ ; CXCR5<sup>int</sup>CD4<sup>+</sup> T cells,  $n = 2$ , T<sub>FH</sub> cells,  $n = 3$ ). Data are representative of or pooled from two independent experiments (**a**, **b**) or representative of four tonsil specimens (**c**, **d**). Graphs depict mean with s.d.



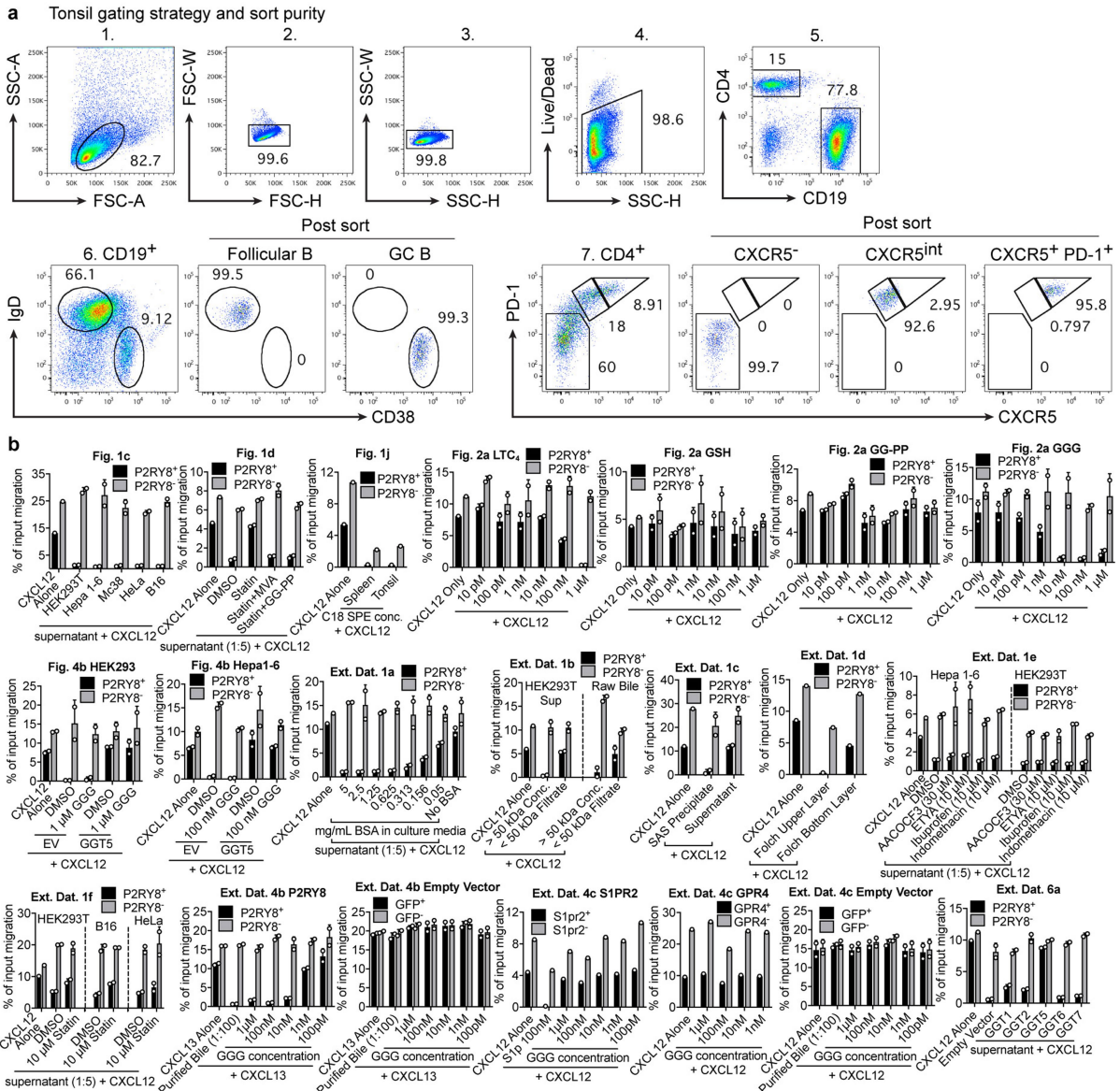
**Extended Data Fig. 7 | GGT5 is expressed by mouse FDCs.** **a**, Violin plots from a single-cell RNA sequencing dataset<sup>18</sup>, showing the relative expression levels of *Ggt1*, *Ggt5*, *Ggt6* and *Ggt7* in the indicated stromal cell (SC) subsets. MRC, marginal reticular cell; PvC, perivascular cell; TRC, T zone reticular cell. **b**, qPCR for expression of *Ggt1*, *Ggt5*, *Ggt6* and *Ggt7* in whole spleen tissue or spleen stroma, relative to *Hprt* ( $n = 3$  biological replicates). **c**, **d**, RNAscope detection of *Ggt5* mRNA (red) counterstained with IgD (brown) in the indicated tissues (spleen, peripheral lymph nodes (LN) and Peyer's patch) in mice eight days after immunization

with SRBCs (**c**) or in lymph nodes from mice treated with LT $\beta$ R-Fc and TNFR-Fc fusion proteins or control IgG for four days (**d**). Serial sections are stained for CR1 (blue) and IgD (brown). Scale bars, 100  $\mu$ m. Each point in **b** corresponds to a biological replicate. Data are representative of five (**c**), two (**d**) or one (**a**) biological replicates per condition. Graphs depict mean with s.d. The violin plots in **a** were generated by a webtool (<http://scorpio.ucsf.edu/shiny/LNSC/>) that does not display the exact minimum, maximum, centre, percentiles or  $n$  numbers for each group.



**Extended Data Fig. 8 | Controls for transduced B cell co-transfer experiments.** **a**, Immunofluorescence images tracking the positioning of adoptively transferred B cells overexpressing empty vector-GFP (green), and co-transferred with either empty vector-Thy1.1- or GGT5-Thy1.1-overexpressing B cells, in unimmunized (top) or SRBC-immunized (bottom) mice, relative to endogenous B cells (IgD, blue). **b**, Quantification of images of the type in **a** and in Fig. 4h, measuring the average distance (in arbitrary units, A.U.) of GFP<sup>+</sup> cells from the centre of B cell follicles using IMARIS software. Each point represents a B cell follicle, and three

to four similarly sized follicles were chosen randomly from three mice per condition ( $n = 10$  follicles per condition). Graph depicts mean with s.d.  $P$  values determined by one-way ANOVA with Bonferroni's multiple comparisons test. **c**, Immunofluorescence images tracking positioning of adoptively transferred B cells overexpressing GGT5 or an empty vector control construct from immunized mice of the type in Fig. 4h, by staining for Thy1.1 (red) relative to endogenous B cells (IgD, blue). Scale bars, 100  $\mu\text{m}$ . Data are representative of three (**a**, **c**) biological replicates per condition.



**Extended Data Fig. 9 | FACS gating strategy and purity. a,** Flow cytometry plots showing the gating scheme that was used to sort the indicated cell subsets from human tonsil, along with post-sort purity. **b,** For each bioassay performed, representative experiments are graphed as percentage of input migration (that is, the percentage of input cells that migrated) for both the transduced and untransduced WEHI-231 subsets

indicated. For Fig. 1j, the C18 SPE concentrates exhibited inhibition of overall migration, probably owing to slight toxicity; however, P2RY8<sup>+</sup> cells were more selectively inhibited than P2RY8<sup>-</sup> cells. The baseline migration across experiments differs based on the growth state of the WEHI-231 cells. Graphs depict mean with s.d.

## Reporting Summary

Nature Research wishes to improve the reproducibility of the work that we publish. This form provides structure for consistency and transparency in reporting. For further information on Nature Research policies, see [Authors & Referees](#) and the [Editorial Policy Checklist](#).

### Statistical parameters

When statistical analyses are reported, confirm that the following items are present in the relevant location (e.g. figure legend, table legend, main text, or Methods section).

n/a Confirmed

- The exact sample size ( $n$ ) for each experimental group/condition, given as a discrete number and unit of measurement
- An indication of whether measurements were taken from distinct samples or whether the same sample was measured repeatedly
- The statistical test(s) used AND whether they are one- or two-sided  
*Only common tests should be described solely by name; describe more complex techniques in the Methods section.*
- A description of all covariates tested
- A description of any assumptions or corrections, such as tests of normality and adjustment for multiple comparisons
- A full description of the statistics including central tendency (e.g. means) or other basic estimates (e.g. regression coefficient) AND variation (e.g. standard deviation) or associated estimates of uncertainty (e.g. confidence intervals)
- For null hypothesis testing, the test statistic (e.g.  $F$ ,  $t$ ,  $r$ ) with confidence intervals, effect sizes, degrees of freedom and  $P$  value noted  
*Give  $P$  values as exact values whenever suitable.*
- For Bayesian analysis, information on the choice of priors and Markov chain Monte Carlo settings
- For hierarchical and complex designs, identification of the appropriate level for tests and full reporting of outcomes
- Estimates of effect sizes (e.g. Cohen's  $d$ , Pearson's  $r$ ), indicating how they were calculated
- Clearly defined error bars  
*State explicitly what error bars represent (e.g. SD, SE, CI)*

*Our web collection on [statistics for biologists](#) may be useful.*

### Software and code

Policy information about [availability of computer code](#)

Data collection

Mass spectrometry data was collected using Analyst software (ver. 1.6.2) for the AB SCIEX QTRAP 6500 and using MassLynx v4.1 for the Waters XEVO-G2 XS QTOF. BD FACSDiva software (LSR II) and BD CellQuest Pro software (FACS Calibur) were used to collect flow cytometry data.

Data analysis

Prism software (ver 7.0e) was used for statistical tests, and Flowjo software (ver 9.7.6) was used to analyze flow cytometry data. IMARIS (ver. 7.4.2) was used to quantify immunofluorescence images.

For manuscripts utilizing custom algorithms or software that are central to the research but not yet described in published literature, software must be made available to editors/reviewers upon request. We strongly encourage code deposition in a community repository (e.g. GitHub). See the Nature Research [guidelines for submitting code & software](#) for further information.

## Data

Policy information about [availability of data](#)

All manuscripts must include a [data availability statement](#). This statement should provide the following information, where applicable:

- Accession codes, unique identifiers, or web links for publicly available datasets
- A list of figures that have associated raw data
- A description of any restrictions on data availability

The data that support the findings of this study are available from the corresponding author upon reasonable request. Source data is provided with the paper for experiments involving animal models or tonsil specimens, including Fig 1i, 1j, 2b, 2c, 3e, and Extended Data Fig 5a, 6e, 7b, 8b.

## Field-specific reporting

Please select the best fit for your research. If you are not sure, read the appropriate sections before making your selection.

Life sciences  Behavioural & social sciences  Ecological, evolutionary & environmental sciences

For a reference copy of the document with all sections, see [nature.com/authors/policies/ReportingSummary-flat.pdf](https://www.nature.com/authors/policies/ReportingSummary-flat.pdf)

## Life sciences study design

All studies must disclose on these points even when the disclosure is negative.

Sample size	Sample sizes were chosen based on our previous experience in the design of experiments of the type in this study, which have yielded reproducible results.
Data exclusions	No data were excluded.
Replication	Findings were reproduced in independent experiments.
Randomization	Samples / organisms were randomized.
Blinding	The investigators were not blinded to group allocation during data collection or analysis. This approach is considered standard for experiments of the type performed in this study.

## Reporting for specific materials, systems and methods

### Materials & experimental systems

n/a	Involvement in the study
<input type="checkbox"/>	<input checked="" type="checkbox"/> Unique biological materials
<input type="checkbox"/>	<input checked="" type="checkbox"/> Antibodies
<input type="checkbox"/>	<input checked="" type="checkbox"/> Eukaryotic cell lines
<input checked="" type="checkbox"/>	<input type="checkbox"/> Palaeontology
<input type="checkbox"/>	<input checked="" type="checkbox"/> Animals and other organisms
<input type="checkbox"/>	<input checked="" type="checkbox"/> Human research participants

### Methods

n/a	Involvement in the study
<input checked="" type="checkbox"/>	<input type="checkbox"/> ChIP-seq
<input type="checkbox"/>	<input checked="" type="checkbox"/> Flow cytometry
<input checked="" type="checkbox"/>	<input type="checkbox"/> MRI-based neuroimaging

## Unique biological materials

Policy information about [availability of materials](#)

Obtaining unique materials

## Antibodies

Antibodies used

For flow cytometry: FITC-conjugated anti-human CD4 (RPA-T4, 35-0049-T100), PE-conjugated anti-human CXCR5 (MU5UBEE, 12-9185-41, ThermoFisher/eBioscience), PerCP-Cy5.5-conjugated anti-human CD38 (HIT2, 303518, Biolegend) PE-Cy7-conjugated anti-human CD19 (HIB19, 302216, Biolegend), APC-conjugated anti-human IgD (IA6-2, 348221, Biolegend), PE-conjugated anti-human IgD (IA6-2, 348203, Biolegend), Pacific Blue-conjugated anti-human PD-1 (EH12.2H7, 329916,

Biolegend), PE-conjugated anti-CD90.1/Thy1.1 (OX-7, 202524, Biolegend), A647-conjugated anti-CD90.1/Thy1.1 (OX-7, 202508, Biolegend), rabbit anti-pAKT (Ser 473, clone D9E, 4060L, Cell Signaling Technology), APC-conjugated goat anti-rabbit IgG (sc-3846, Santa Cruz Biotechnologies), AF647-conjugated goat anti-rabbit IgG (A-21245, Invitrogen), anti-mouse CD180 (clone RP/14, BD). The OX56 antibody was produced via hybridoma and conjugated to biotin.

For immunohistochemistry: polyclonal rabbit anti-human GGT5 (PA5-52514, Thermo), polyclonal rabbit anti-human P2RY8 (Sigma - Atlas Antibodies, HPA003631) goat anti-mouse IgD (GAM/IGD(FC)/75, Cedarlane Laboratories), AF647-conjugated streptavidin (S21374, Invitrogen), AMCA-conjugated donkey anti-goat IgG (705-156-147, Jackson ImmunoResearch), biotin-conjugated anti-Thy1.1 (HIS51, 13-0900-85, eBioscience), A488-conjugated rabbit anti-GFP (A21311, Thermo), biotin-conjugated anti-CD35 (8C12, 553816, BD), alkaline phosphatase (AP)-conjugated streptavidin (016-050-084, Jackson ImmunoResearch), HRP-conjugated donkey anti-goat IgG (705-035-147, Jackson ImmunoResearch), biotin-conjugated anti-human CD4 (Biolegend, RPA-T4), AF555-conjugated streptavidin (S-21381, Invitrogen), Cy3-conjugated streptavidin (016-160-084, Jackson ImmunoResearch), biotin-conjugated anti-human CD21 (Biolegend, clone Bu32, 354913), HRP-conjugated donkey anti-rabbit IgG (711-035-152, Jackson ImmunoResearch), HRP-conjugated streptavidin (016-030-084, Jackson ImmunoResearch), AF647-conjugated goat anti-rabbit IgG (A-21245, Invitrogen).

#### Validation

Antibodies were purchased from widely used vendors which performed validation. Our lab also validates antibodies by comparing their staining profiles with publications that have used the same clone. Aside from those described below, the antibodies used in this study are commonly used by the field. The OX56-biotin antibody was validated by staining cells overexpressing either an OX56-tagged receptor or an untagged version of the same receptor, which showed only positive staining for cells overexpressing the OX56-tagged version of the receptor. The OX56 epitope is described in Cyster et al., EMBO J, 1991. Anti-P2RY8 antibody staining specificity was validated by staining empty-vector or P2RY8-transduced WEHI-231 cells, which showed that only the P2RY8-expressing WEHI-231 cells stained positively (see Extended Data Fig 5c for validation data).

## Eukaryotic cell lines

Policy information about [cell lines](#)

#### Cell line source(s)

HEK293T, Hepa 1-6, HeLa, B16, MC38, WEHI-231, M12, PLAT-E, Ly7, Ly8, and DOHH2 were previously obtained from other laboratories.

#### Authentication

Aside from morphological inspection, the cell lines used were not further authenticated.

#### Mycoplasma contamination

The cell lines were not tested for mycoplasma contamination.

#### Commonly misidentified lines (See [ICLAC](#) register)

No commonly misidentified lines were used in the study.

## Animals and other organisms

Policy information about [studies involving animals](#); [ARRIVE guidelines](#) recommended for reporting animal research

#### Laboratory animals

C57BL/6J mice were bred in an internal colony and mice of both sexes were used between 7 and 12 weeks of age. CD19<sup>-/-</sup> mice on a B6 background were from Jax and mice of both sexes were used between 7 and 12 weeks of age.

#### Wild animals

The study did not involve wild animals.

#### Field-collected samples

The study did not involve field-collected samples.

## Human research participants

Policy information about [studies involving human research participants](#)

#### Population characteristics

We received de-identified human tonsil specimens from the UCSF Biospecimen Resources Program. No patient information was provided, so the population characteristics are unknown.

#### Recruitment

A calendar was provided by the UCSF Biospecimen Resources Program listing tonsillectomy surgery dates, from which we requested de-identified tonsil specimens. No patient information was provided, aside from the time of surgery.

## Flow Cytometry

### Plots

Confirm that:

- The axis labels state the marker and fluorochrome used (e.g. CD4-FITC).
- The axis scales are clearly visible. Include numbers along axes only for bottom left plot of group (a 'group' is an analysis of identical markers).
- All plots are contour plots with outliers or pseudocolor plots.
- A numerical value for number of cells or percentage (with statistics) is provided.

## Methodology

Sample preparation	For bioassays and internalization assays, cells were obtained from cultured cell lines. Human tonsil cells were obtained from fresh, de-identified tissue specimens by mashing through a 100 micron metal mesh. Detailed preparation of these cells is listed in the methods section. For staining, cells were placed into 96-well round bottom plates and washed in flow cytometry buffer (PBS containing 2% FBS and 0.1% sodium azide and 1 mM EDTA). For cell sorting, cells were stained on ice in RPMI containing 2% FBS and 10 mM HEPES.
Instrument	BD LSR II flow cytometer, BD FACS Calibur flow cytometer, BD FACSAriaII cell sorter
Software	BD FACSDiva software (LSR II) and BD CellQuest Pro software (FACS Calibur) were used to collect flow cytometry data. Flowjo (ver 9.7.6) was used to analyze flow cytometry data.
Cell population abundance	Examples of human tonsil cell population abundance are provided in Extended Data Figure 9a. WEHI-231 cells were sorted for the top 5% highest GFP+ cells. These cells were mixed with untransduced cells from the initial culture. Examples of this mixture are present in the manuscript.
Gating strategy	For virally-transduced WEHI231 and M12 cell lines, cells were gated by reporter (GFP or Thy1.1) expression by selecting all of the reporter positive cells. Examples are included in the Figures of the manuscript. The gating strategy and post-sort purity for human tonsil cell populations is provided in Extended Data Figure 9a. For internalization assays, OX56 surface levels on transduced cells were assessed by drawing a gate on the top ~40% of OX56-expressing cells in the control condition, then using the same gate on the transduced cells treated with various compounds to assess internalization.

Tick this box to confirm that a figure exemplifying the gating strategy is provided in the Supplementary Information.